CHAPTER - 5

RESULTS AND DISCUSSION

5.1 Pt-Co(3:1)/C_{AB} cathode electrocatalyst performance evaluation: Part I

5.1.1 Physical Characterization

5.1.1.1 X-ray diffraction (XRD) analysis

The crystallographic properties of all three synthesized Pt-Co/C_{AB} electrocatalysts were measured by the XRD analysis. The XRD pattern of all three synthesized electrocatalysts are shown in Figure 5.1. In the present XRD analysis, the peak of Pt (220) was selected for the determination of lattice parameters of synthesized electrocatalyst because this peak is far from the background effect of the electrocatalyst support material i.e., C_{AB} (Table 5.1) (Hyun et al., 13 and Lima et al., 2006). As per the standard of JCPDS 04-0802 file of platinum facets of face-centered-cubic, the strong diffraction peaks at the Bragg angles of 67.45° is corresponding to the (220) plane (Choudhary and Pramanik 2020a). It is clearly seen in the Figure 5.1 that the Pt-Co/C_{AB}-DMSO, Pt-Co/C_{AB}-DMF, Pt-Co/C_{AB}-EG and Pt-Co/C_{AB}-W alloy electrocatalyst show their prominent diffraction peak for Pt at around 2θ of 67.31°, 68.20°, 69.33° and 67.59°, respectively of face-centered cubic (FCC) structure at the plane of (220). The highest shifting of diffraction peak in XRD pattern at (220) plane was observed for the Pt-Co/C_{AB}-EG electrocatalyst i.e., 2θ of 67.45° for pure Pt to 69.33° when alloy of Pt-Co was formed using solvent EG. The XRD diffraction characteristics have been enlarged for the plane Pt (220) to have a clear view of the highest shifting of the peak at the plane (220) for the Pt-Co/C_{AB}-EG electrocatalyst which is presented in the Appendix B. This prominent shifting of 2θ proved the incorporation of Co into Pt metal of FCC structure, which results in alloy formation of Pt-Co/C_{AB}.

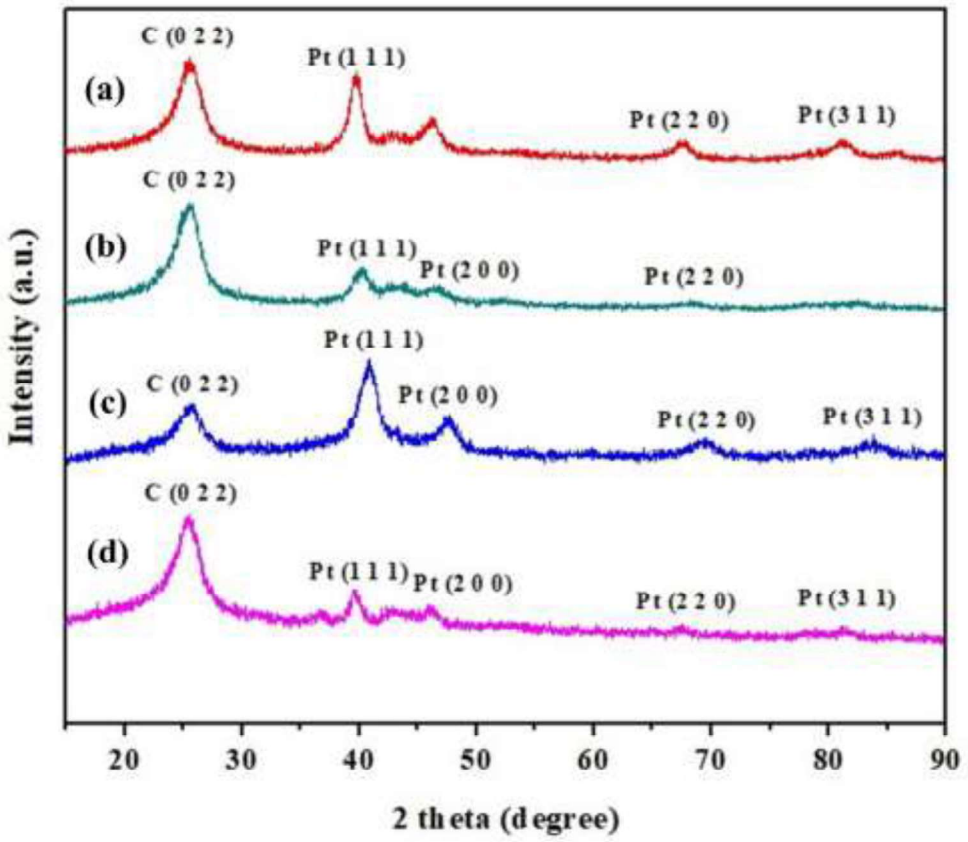

FIGURE 5.1 XRD pattern of Pt-Co/C_{AB} synthesized electrocatalysts (a) Pt-Co/C_{AB}-DMSO, (b) Pt-Co/C_{AB}-DMF, (c) Pt-Co/C_{AB}-EG and Pt-Co/C_{AB}-W.

Table 5.1 Lattice parameters and the particle size at Pt (220) X-ray diffraction peak of Pt-Co/C_{AB} synthesized electrocatalyst.

Electrocatalyst Types	2θ (°)	d-value (nm)	Lattice parameter (nm)	Crystallize size (d_c) (nm)	Alloying degree (%)
Pt-Co/C_{AB}-DMSO	67.31	0.1389	0.3929	5.70	3.26
Pt-Co/C_{AB}-DMF	68.20	0.1373	0.3884	3.70	8.97
Pt-Co/C_{AB}-EG	69.33	0.1353	0.3829	3.49	26.36
Pt-Co/C_{AB}-W	67.59	0.1384	0.3916	5.12	0.27
Pt/C (JCPDS 04-0802)	67.45	0.1386	0.3923	–	–

The lattice parameter was also found to be a little lower (0.3829 nm) for the Pt-Co/C_{AB}-EG electrocatalyst synthesized with ethylene glycol as the solvent. It indicates the formation of ordered robust metal solutions/alloy of Pt-Co/C_{AB}-EG electrocatalysts (Choudhary and Pramanik 2019). The presence of pure Co or its oxides cannot be ignored and it may be due to the presence of the little amount of amorphous phase (Singh and Pramanik 2019). The lattice parameter of the Pt-Co/C_{AB}-DMSO, Pt-Co/C_{AB}-DMF and Pt-Co/C_{AB}-W metal-alloys electrocatalysts were 0.3929 nm, 0.3884 nm and 0.3916 nm, respectively against the lattice parameter of pure, noble metal Pt (bulk) of 0.3923 nm (Safo and Oezaslan 2017). The mean crystallite sizes (d_c) calculated by Scherrer's formula (Equation (5.1)) for synthesized electrocatalysts Pt-Co/C_{AB}-DMSO, Pt-Co/C_{AB}-DMF, Pt-Co/C_{AB}-EG and Pt-Co/C_{AB}- W were 5.70 nm, 3.70 nm, 3.49 nm and 10.50 nm, respectively (Safo and Oezaslan 2017; Zahari and Aziz 2012).

The d-spacing was calculated using Bragg's equation (Equation 5.2) corresponding to Pt (220) plane for the electrocatalyst synthesized from ethylene glycol (Pt-Co/C_{AB}-EG) was 0.1353 nm, which is lowest among all synthesized electrocatalysts (Safo and Oezaslan 2017; Zahari and Aziz 2012).

$$d_c = \frac{0.9\lambda}{\beta\cos\theta} \tag{5.1}$$

$$n\lambda = 2d_{nkl}\sin\theta \tag{5.2}$$

Where, d_c is calculated crystallite size, λ is X-ray wavelength (0.154 nm), β is the width of the peak (in radius) and θ is the angle at peak position, n is the order of diffraction, d_{hkl} is the interplanar distance between two planes of miller index (hkl). It is reported in the literature that there is a contraction in the lattice parameter (JCPDS 04-0802 file) and hence, a decrease in Pt-Pt bond distance (Antolini et al., 2005 and Lima et al., 2006). The electrocatalytic activity of the

synthesized Pt-Co/C_{AB} cathode electrocatalyst might be enhanced by the incorporation of Co in the Pt and forming Pt-Co alloy. The alloying percentage of Co in the Pt-Co/C_{AB} electrocatalyst was calculated using Vegard's law (Equation 5.3) (Lima et al., 2006). It is assumed that the dependence of the lattice parameter on Co content is the same for supported and unsupported Pt-Co alloys.

$$x_{alloy} = \frac{a - a_o}{k} \tag{5.3}$$

Where, x_{alloy} is the atomic fraction of Co in carbon supported Pt-Co alloy, a is the Pt-Co alloy lattice parameter, a_o is the lattice parameter of pure carbon supported Pt (0.3917 nm), and k = 0.0368 nm is constant, obtained from the lattice parameter of unsupported Pt (0.3923 nm) and Pt_3Co alloy (0.3831 nm), assuming a linear dependence with the atomic fraction (Lima et al., 2006). The % Co in the alloy was found 0.27 % in the Pt-Co/C_{AB}-W electrocatalyst i.e., lowest. On the other side, the % alloying of Co in the Pt-Co/C_{AB}-EG electrocatalyst was found to be 26.36 %, which is the highest among all synthesized Pt-Co/C_{AB} electrocatalyst (Table 5.1). Thus, it is expected that the cathode electrocatalyst Pt-Co/C_{AB}-EG may exhibit better electronic activity in half-cell and single cell for ORR (Salgado et al., 2004 and Santiago et al., 2007).

5.1.1.2 Scanning electron microscopy (SEM) analysis

The studies on the surface morphology of Pt-Co/C_{AB} synthesized electrocatalysts were carried out using scanning electron microscopy. It is seen from the Figure 5.2(a-d) that synthesized electrocatalysts Pt-Co/C_{AB}-DMSO, Pt-Co/C_{AB}-DMF, Pt-Co/C_{AB}-EG and Pt-Co/C_{AB}-W were spherical in shape and nano-range in size (Choi et al., 2021 and Pramanik et al., 2008). The best performance of electrocatalysts can be achieved by optimizing the particle size of the synthesized electrocatalyst. As the particle size of the electrocatalyst decreases, the available active surface

area gradually increases. The synthesized electrocatalyst Pt-Co/C_{AB}-EG (Figure 5.2c) produced a more uniform surface morphology of Pt and Co alloy as compared to the other three synthesized electrocatalysts i.e., Pt-Co/C_{AB}-DMSO, Pt-Co/C_{AB}-DMF and Pt-Co/C_{AB}-W (Bard et al., 2022). A little contrast of white spots was observed in the electrocatalyst Pt-Co/C_{AB}-DMSO, Pt-Co/C_{AB}-DMF and Pt-Co/C_{AB}-W, which may be due to the charging of Co particles (Tayal et al., 2011).

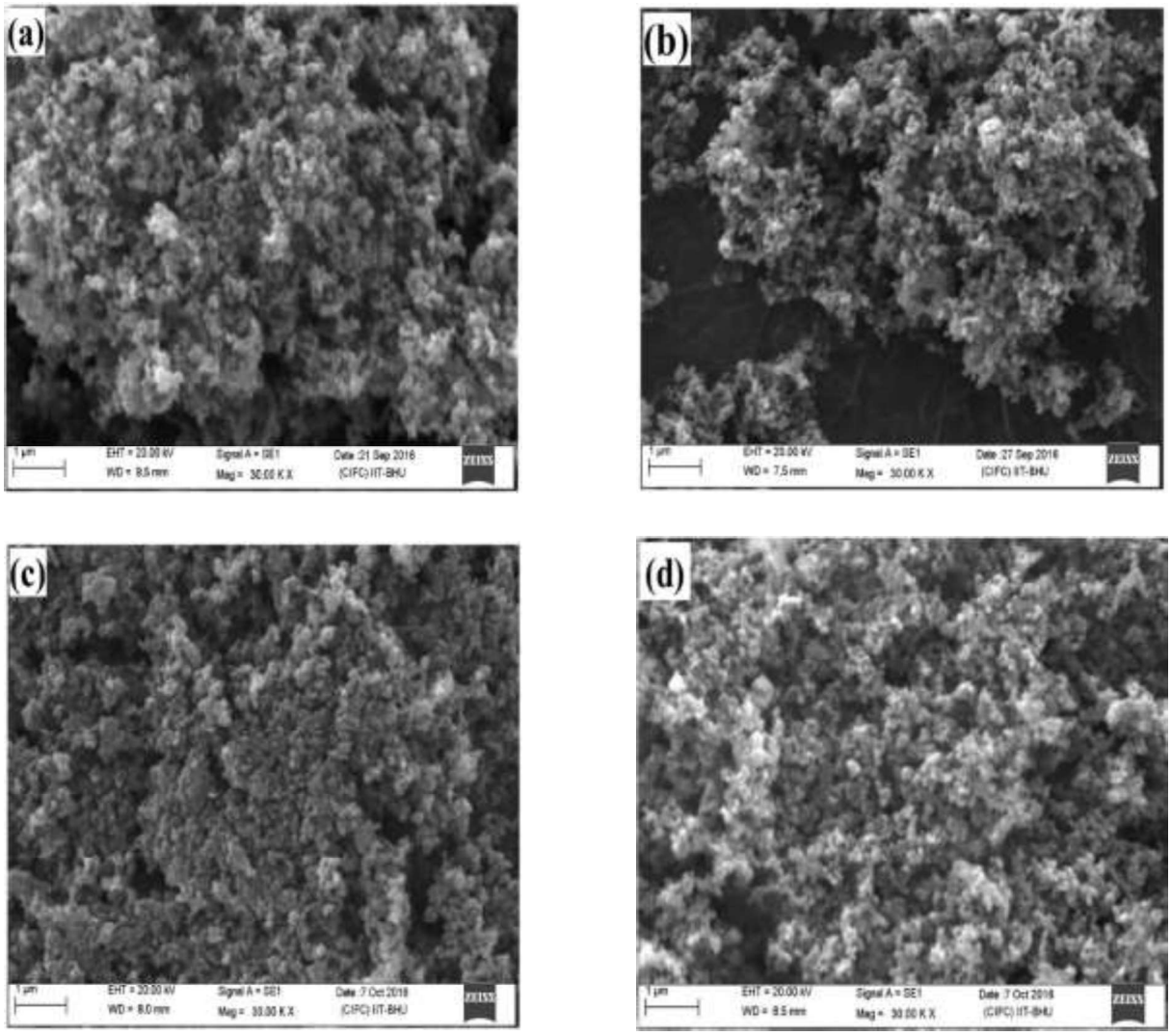

Figure 5.2 SEM images of Pt-Co/C_{AB} synthesized electrocatalyst (a) Pt-Co/C_{AB}-DMSO, (b) Pt-Co/C_{AB}-DMF, (c) Pt-Co/C_{AB}-EG and (d) Pt-Co/C_{AB}-W.

5.1.1.3 Energy dispersive X-ray (EDX) analysis

The surface composition of all active elements and elemental mapping were performed by EDX analysis which shows the strong presence of C, Pt and Co elements in every synthesized electrocatalyst Pt-Co/C_{AB}-DMSO, Pt-Co/C_{AB}-DMF, Pt-Co/C_{AB}-EG and Pt-Co/C_{AB}-W (Figure (3a-d)). The elemental mapping of synthesized Pt-Co/C_{AB}-DMSO, Pt-Co/C_{AB}-DMF, and Pt-Co/C_{AB}-EG electrocatalysts by EDX using different color code for various elements like Pt, Co, O and C are represented in Appendix C (Figure C(1-3)). It is clearly seen in Figure C(1-3) that the metal elements are uniformly distributed in the synthesized electrocatalyst. The highest peaks of acetylene black carbon were observed due to the strong presence of C_{AB} support material. The elemental compositions of all Pt-Co/C_{AB} electrocatalysts were analyzed by EDX and presented in Table 5.2 with nominal composition. The desired metal loading (Pt) was not in good agreement with the nominal composition of Pt-Co/C_{AB} electrocatalyst because Pt might be penetrated in the pores of agglomerated support material i.e., C_{AB}. Also, slightly change in actual metal loading could be associated with the metal losses in separation and purification processes (Shen et al., 2015b). A little amount of oxygen was observed due to its presence in the testing surrounding (Castagna et al., 2019). There was a little variation in elemental compositions of the prepared electrocatalysts from the nominal composition. It may be due to the heterogeneous surface formation of the synthesized electrocatalyst and the selection of spectrum in the EDX images. Whereas, elemental mapping with different colour codes in Appendix C (Figure C1 to Figure C3), shows the highest amount of Pt metal (20 wt. %) which is similar to the nominal composition of Pt metal.

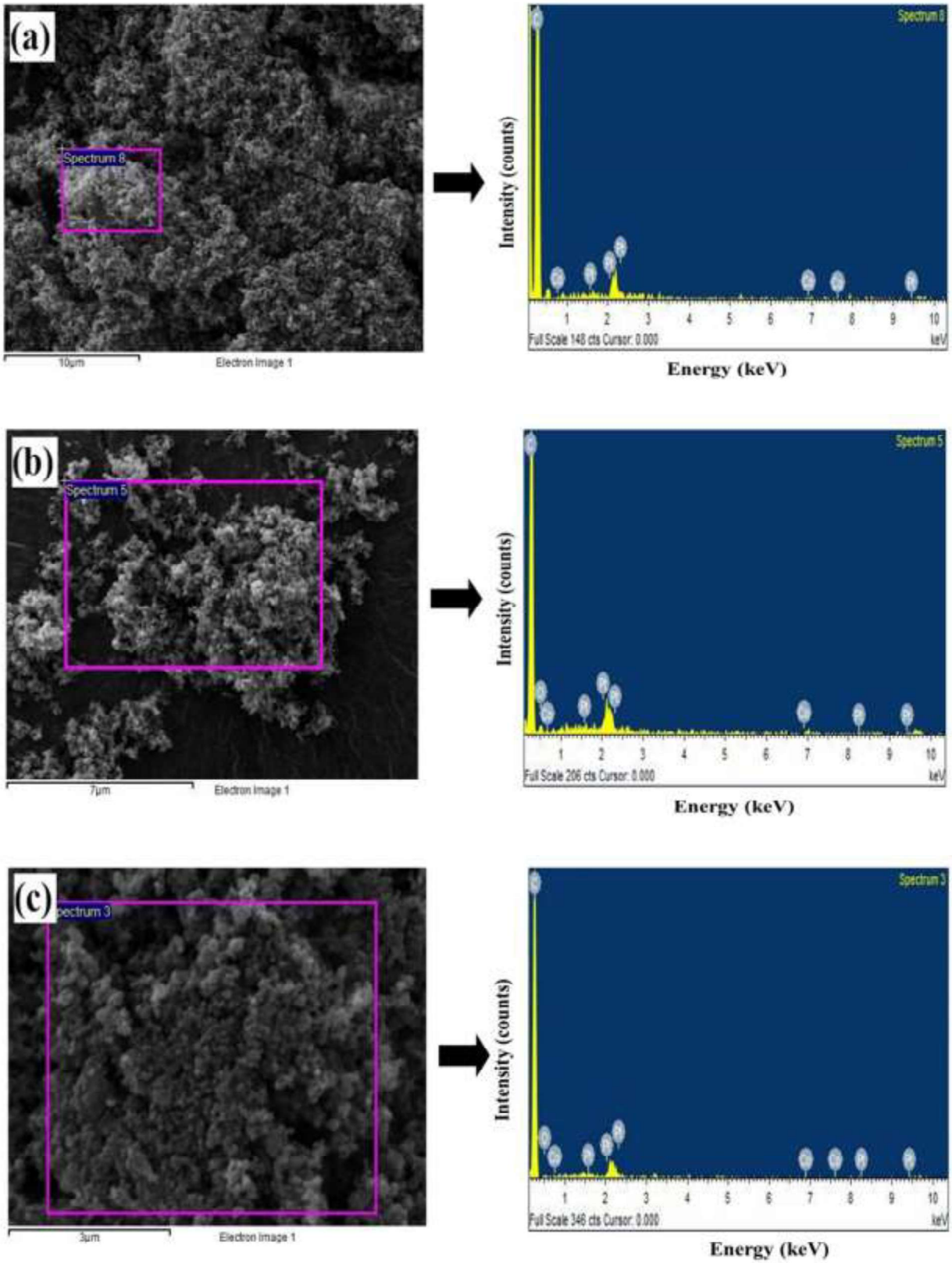
(a)
Spectrum 8
10µm
Electron Image 1
Spectrum 8
Intensity (counts)
Full Scale 148 cts Cursor: 0.000
keV
Energy (keV)
(b)
Spectrum 5
7µm
Electron Image 1
Spectrum 5
Intensity (counts)
Full Scale 206 cts Cursor: 0.000
keV
Energy (keV)
(c)
pectrum 3
3µm
Electron Image 1
Spectrum 3
Intensity (counts)
Full Scale 346 cts Cursor: 0.000
keV
Energy (keV)

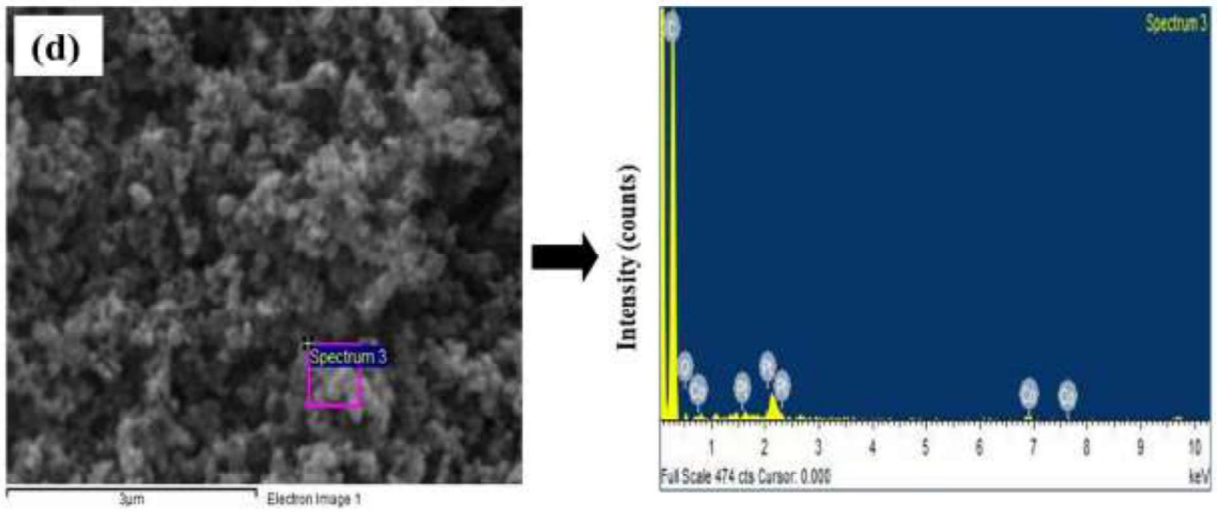

Figure 5.3 EDX images of Pt-Co/C_{AB} synthesized electrocatalyst (a) Pt-Co/C_{AB}-DMSO, (b) Pt-Co/C_{AB}-DMF, (c) Pt-Co/C_{AB}-EG and (d) Pt-Co/C_{AB}-W respectively.

Table 5.2 Surface concentration of synthesized electrocatalyst obtained from EDX analysis.

Electrocatalyst type	EDX composition			Nominal composition		
	Pt (wt.%)	Co (wt.%)	C (wt.%)	Pt (wt.%)	Co (wt.%)	C (wt.%)
Pt-Co/C_{AB}-DMSO	9.01	1.05	89.94	18.17	1.83	80
Pt-Co/C_{AB}-DMF	9.45	1.25	89.30	18.17	1.83	80
Pt-Co/C_{AB}-EG	10.24	1.13	88.63	18.17	1.83	80
Pt-Co/C_{AB}-W	10.10	1.01	88.89	18.17	1.83	80

5.1.1.4 Transmission electron microscopy (TEM) analysis

Figure 5.4(a-d) show the TEM images and respective histograms which give the information about the particle size distribution, shape and size of all four of synthesized Pt-Co/C_{AB} electrocatalysts. The mean particle size of synthesized nanoparticles were measured using Image J software by selecting 75 spherical dark black metal alloy particles which are distributed over electrocatalyst support C_{AB} for all four TEM images separately (Figure 5.4(a-d)) (Castagna et al., 2019). The size of electrocatalyst support material (C_{AB}) was found in range of 35-55 nm (Pramanik et al., 2008 and Hyun et al., 2013). After analysis of all these TEM images, it was also observed that the

particle size varies from 4 to 20 nm, 5 to 16 nm, 2 to 6 nm, and 2 to 12 nm with an average particle size of 10.71 ± 3.06 nm, 9.74 ± 2.30 nm, 4.18 ± 1.04 nm and 7.08 ± 1.98 nm for the synthesized cathode nano-range electrocatalyst Pt-Co/C_{AB}-DMSO, Pt-Co/C_{AB}-DMF, Pt-Co/C_{AB}-EG and Pt-Co/C_{AB}-W, respectively (Table 5.3 and Table 5.4). The mean particle size of electrocatalyst Pt-Co/C_{AB}-DMSO, Pt-Co/C_{AB}-DMF and Pt-Co/C_{AB}-W have a little larger particle size as compared to synthesized electrocatalyst Pt-Co/C_{AB}-EG due to agglomeration of Pt-Co metal alloy in the first two types of electrocatalyst. It is also observed from the comparison of the four TEM micrographs that the Pt-Co/C_{AB}-EG nanoparticles were dispersed uniformly over carbon support. A difference in particle size was obtained between XRD and TEM analysis because XRD displays crystalline particles rather than real morphology (Panjiara and Pramanik 2021). However, the trend of particle size in TEM analysis was found (Table 5.3) which is similar to that of XRD analysis (Table 5.1). Similar to XRD analysis, TEM analysis results of all four synthesized electrocatalysts also confirm that Pt-Co/C_{AB}-EG would obviously resulting in best performance in half-cell and single cell test.

Table 5.3 The average particle size of electrocatalysts from TEM analysis and comparison with XRD average crystallite size.

Electrocatalysts Type	**Average particle size by TEM (nm)**	**Average particle size by XRD (nm)**
Pt-Co/C_{AB}-DMSO	10.71 ± 3.06	5.70
Pt-Co/C_{AB}-DMF	9.74 ± 2.30	3.70
Pt-Co/C_{AB}-EG	4.18 ± 1.04	3.49
Pt-Co/C_{AB}-W	7.08 ± 1.98	5.12

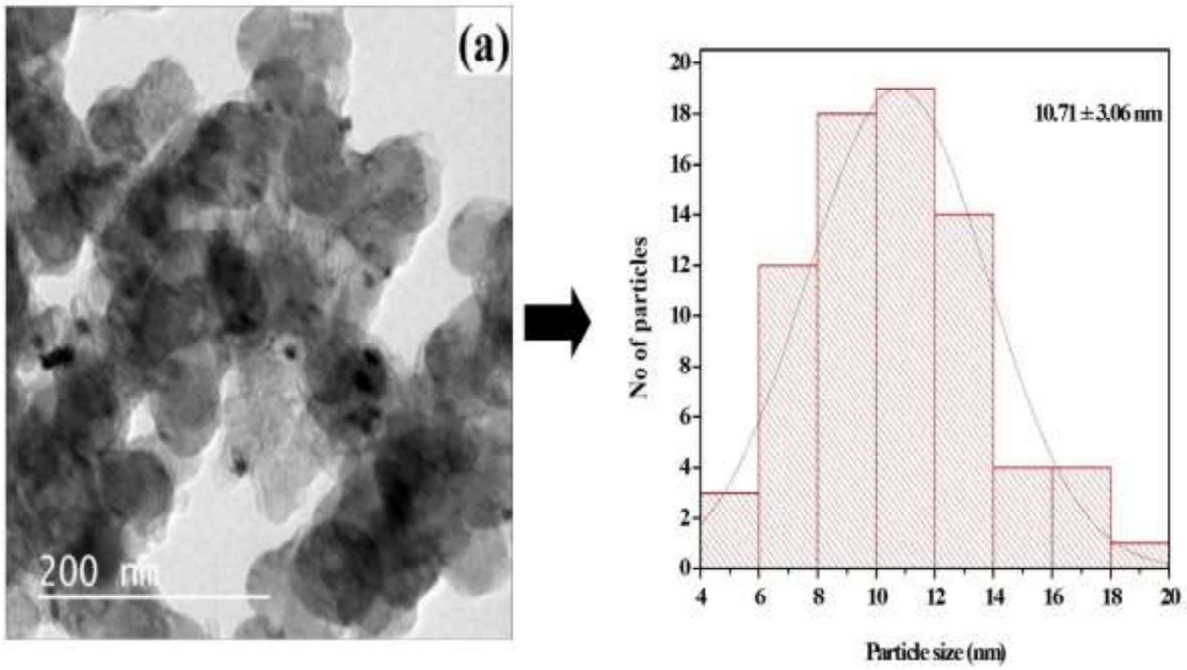
(a)
200 nm
No of particles
Particle size (nm)
10.71 ± 3.06 nm

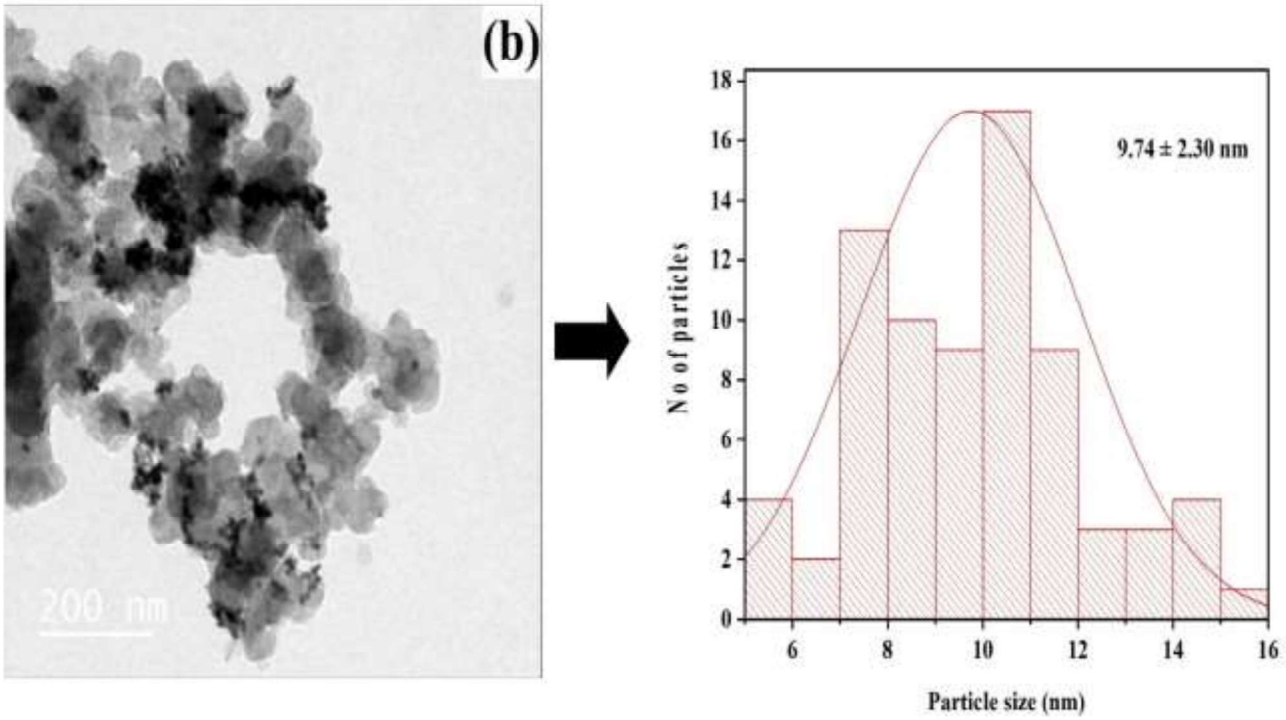
(b)
200 nm
No of particles
Particle size (nm)
9.74 ± 2.30 nm

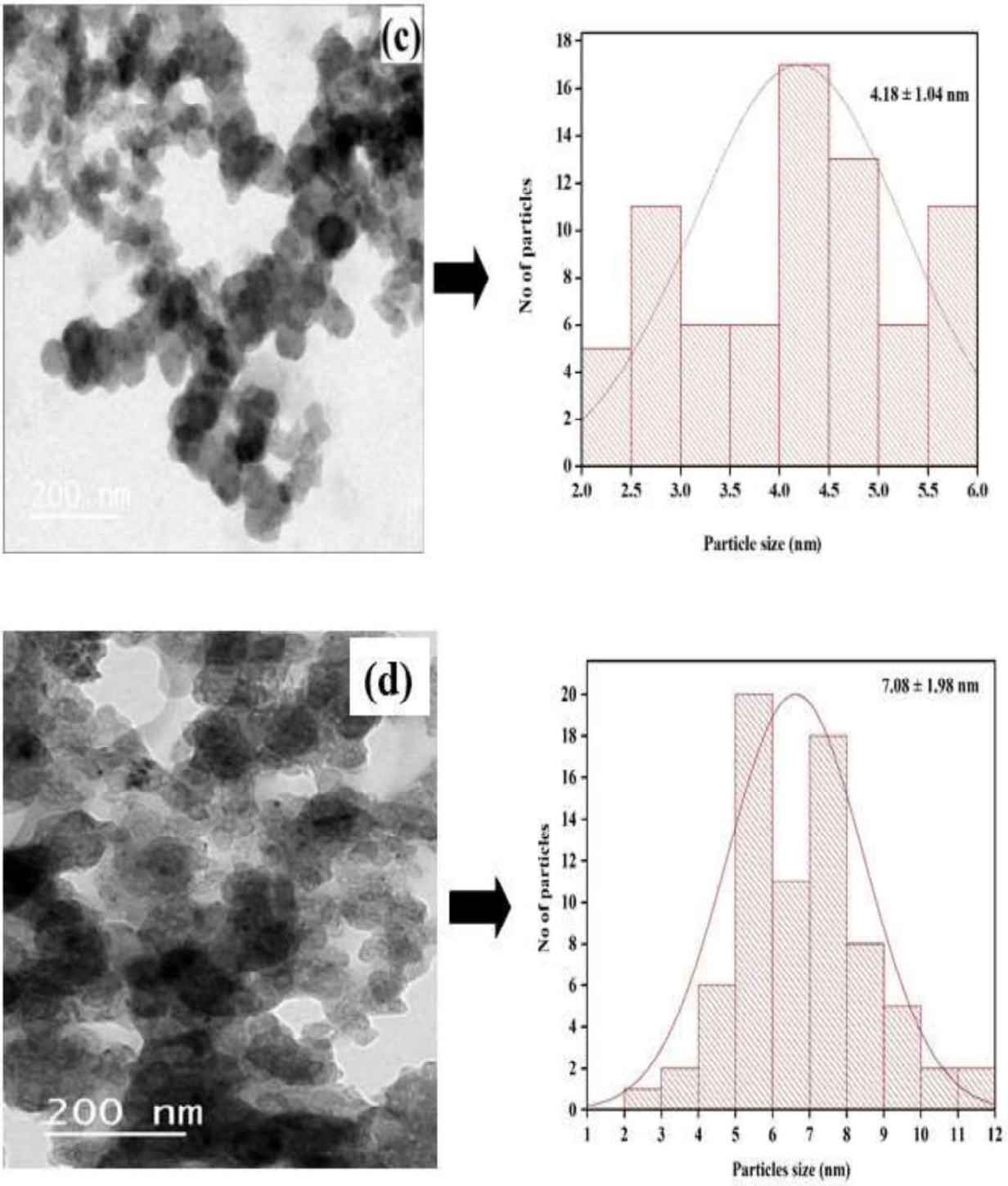

Figure 5.4 TEM image and corresponding histogram of synthesized electrocatalyst (a) Pt-Co/C_{AB}-DMSO, (b) Pt-Co/C_{AB}-DMF, (c) Pt-Co/C_{AB}-EG and (d) Pt-Co/C_{AB}-W respectively.

TABLE 5.4 Particle size distribution of synthesized electrocatalysts by TEM analysis.

Type of electrocatalyst	% of particles number	No. of particles	Particle size (nm)
Pt-Co/C_{AB}-DMSO	4	3	2-6
	16	12	6-8
	24	18	8-10
	25.33	**19**	**10-12**
	18.67	14	12-14
	5.33	4	14-16
	5.33	4	16-18
	1.33	1	18-20
Pt-Co/C_{AB}-DMF	5.33	4	5-6
	2.67	2	6-7
	17.33	13	7-8
	13.33	10	8-9
	12	9	9-10
	22.67	**17**	**10-11**
	12	9	11-12
	4	3	12-13
	4	3	13-14
	5.33	4	14-15
	1.33	1	15-16
Pt-Co/C_{AB}-EG	6.66	5	2-2.5
	14.66	11	2.5-3
	8	6	3-3.5
	8	6	3.5-4
	22.67	**17**	**4-4.5**
	17.33	13	4.5-5
	8	6	5-5.5
	14.67	11	5.5-6
Pt-Co/C_{AB}-W	1.33	1	2-3
	2.66	2	3-4
	8	6	4-5
	26.66	**20**	**5-6**
	14.67	11	6-7
	24	18	7-8
	10.67	8	8-9
	6.67	5	9-10
	2.67	2	10-11
	2.67	2	11-12

5.1.2 Electrochemical characterization

5.1.2.1 Cyclic voltammetry (CV) of cathode electrode

5.1.2.1.1 Effect of scan rate

The oxygen reduction kinetics depends upon the various operating parameters which directly affect the performance of ORR. In multi variable system, the scan rate is one of them, which controls the electrochemical performance of a system. In CV studies of Pt-Co/C_{AB} electrocatalysts, scan rates control the shape and size of oxygen reduction peak by maintaining the thickness of the diffusion layer through which oxygen transport takes place to the cathode electrode surface from bulk phase to the electrocatalyst surface (Figure 5.5(a-d)). The loading of cathode electrocatalysts for all four types of electrocatalysts were maintained at 1 mg/cm^2 as discussed in section 3.4.1 (Page no. 53). The working electrode was immersed in an oxygen saturated electrolyte solution of 0.5 M $HClO_4$. The scan rate was varied from 80 mV/s to 100 mV/s irrespective of electrocatalyst types. Only one oxygen reduction peak was found in a backward scan for all four types of cathode electrodes with the different applied voltage range from –0.30 V to 1.0 V for Pt-Co/C_{AB}-DMSO (Figure 5.5a), −0.8 V to 0.7 V for Pt-Co/C_{AB}-DMF (Figure 5.5b), –0.5 V to 1.30 V for Pt-Co/C_{AB}-EG (Figure 5c) and –0.5 V to 1.50 V for Pt-Co/C_{AB}-W (Figure 5.5d). The single reduction peak in the backward scan confirms that the ORR proceeds through the single step four electron mechanisms as mentioned in equation (Equation 1.8, Page no. 8) for Pt-Co/C_{AB}-DMSO, Pt-Co/C_{AB}-DMF and Pt-Co/C_{AB}-EG electrocatalyst, while two reduction peak in the backward scan confirms that the ORR proceeds through the two step four electron mechanisms for Pt-Co/C_{AB}-W (Equation (1.4) – (1.7)). It is seen from Figure 5(a-d) that the oxygen reduction peak current density increases with the increase in scan rate from 80 mV/s to 100 mV/s for all types of electrocatalysts. The larger size of the oxygen reduction peak indicates the higher amount of oxygen absorbed on

the surface of the cathode electrode and thus, resulting in faster reduction reaction kinetics (Rathoure and Pramanik 2016). As already mentioned, the thickness of the diffusion layer depends upon the voltage scan rate. The thickness of the diffusion layer is large at a low scan rate as sufficient time it gets to develop in comparison to a high scan rate. Thus, oxygen flux available to the cathode surface was low for a slow scan rate of 80 mV/s and 90 mV/s, and high for the highest scan rate of 100 mV/s. Due to this, a higher scan rate of 100 mV/s results in a very high current density irrespective of electrocatalyst types. To maintain consistency, the scan rate of 100 mV/s was selected as the basis for all CV analyses in the preceding sections.

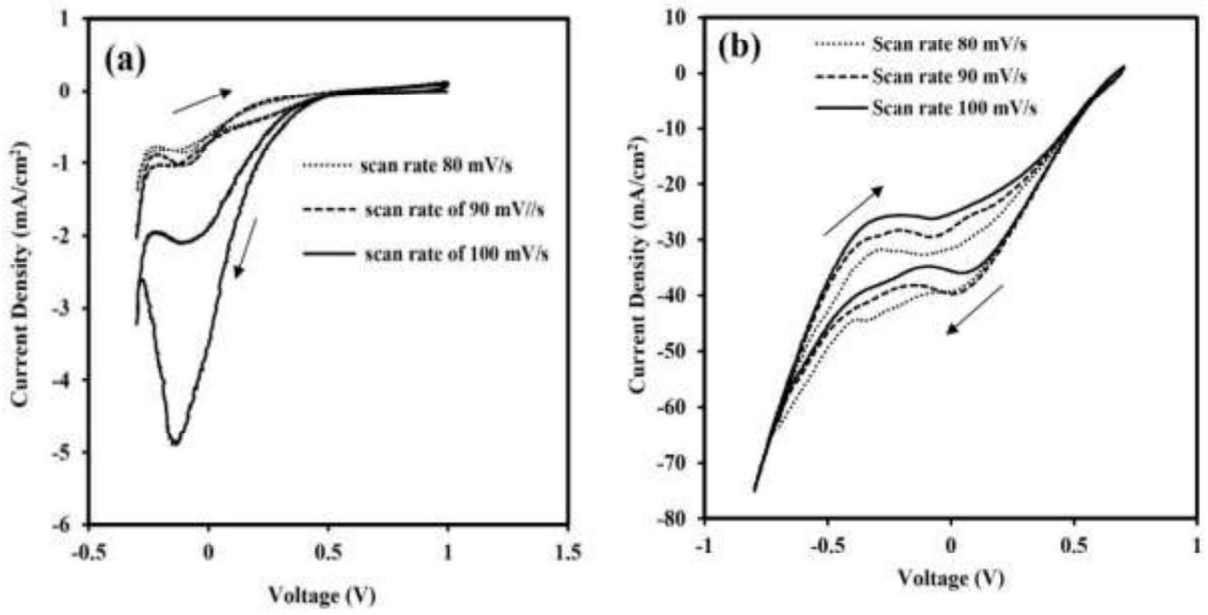

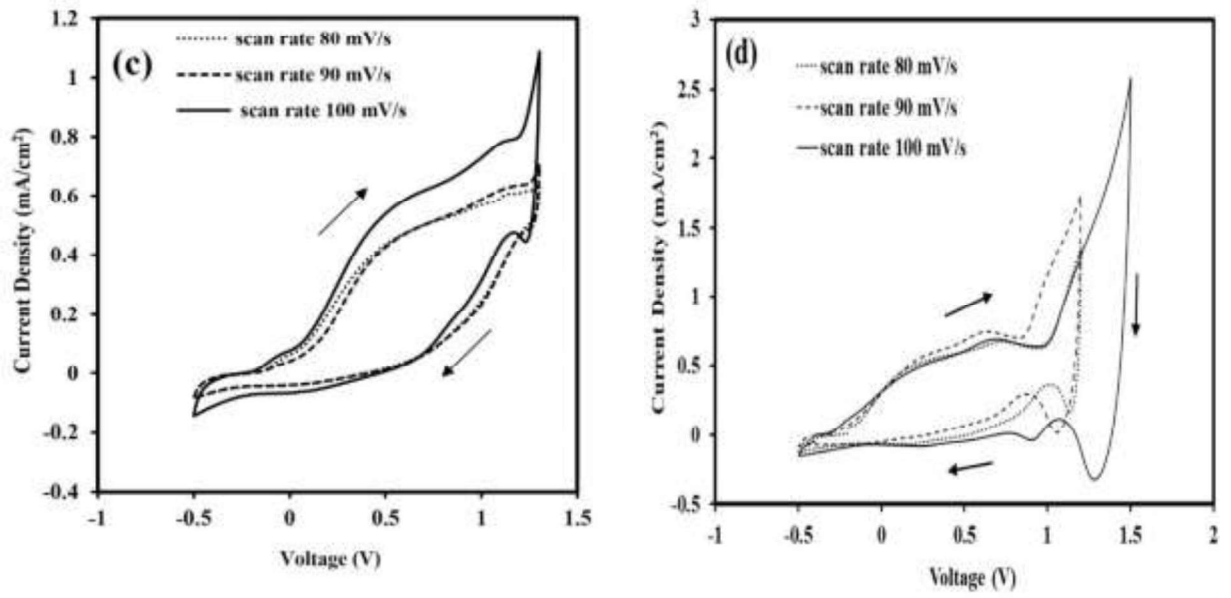

Figure 5.5 Cyclic voltammetry for synthesized electrocatalyst (a) Pt-Co/C_{AB}-DMSO, (b) Pt-Co/C_{AB}-DMF, (c) Pt-Co/C_{AB}-EG and (d) Pt-Co/C_{AB}-W respectively of fixed loading 1 mg/cm^2 with different scan rates using oxygen saturated 0.5 M $HClO_4$ electrolyte.

5.1.2.1.2 CV study of cathode in oxygen and nitrogen purged electrolyte solution

The cyclic voltammograms for ORR were obtained using all four types of synthesized electrocatalysts Pt-Co/C_{AB}-DMSO, Pt-Co/C_{AB}-DMF, Pt-Co/C_{AB}-EG and Pt-Co/C_{AB}-W, respectively at a scan rate of 100 mV/s (Figure 5.6(a-d)). All four types of electrocatalyst, the cathode loading was kept constant at 1 mg/cm^2. The developed electrodes were immersed in nitrogen purged electrolyte solution of 0.5 M $HClO_4$ at a room temperature of 30 ºC to investigate the nature of CVs in an inert atmosphere. The inert atmosphere was maintained by continuous purging of nitrogen for 1 hr through electrolyte solution. Further, all three electrodes were systematically immersed in oxygen saturated solution one after another using similar conditions to study the ORR mechanism in presence of oxidant oxygen. To achieve oxygen saturated electrolyte solution, oxygen was continuously purged for 1 hr. At a constant scan rate of 100 mV/s,

all four types of cathode electrode were also tested for a range of applied voltages, which include 0.30 V to 1.0 V for Pt-Co/C_{AB}-DMSO (Figure 5.6a), 0.80 V to 0.70 V for Pt-Co/C_{AB}-DMF (Figure 5.6b), 0.50 V to 1.30 V for Pt-Co/C_{AB}-EG (Figure 5.6c) and -05 V to 1.50 V for Pt-Co/C_{AB}-W (Figure 5.6d). All the CV characteristics show a single oxygen reduction peak in the backward scan, and those are due to the presence of oxygen in the electrolyte. However, no reduction peak was observed in nitrogen-purged electrolyte solution due to the absence of oxidant oxygen in each analysis (Singh and Pramanik 2019). The oxygen reduction peaks were observed at the peak potential of –0.16 V, 0.11 V, 1.25 V and +0.95 V or +1.32 V having their corresponding peak current densities of 4.80 mA/cm^2, 34.86 mA/cm^2, 0.445 mA/cm^2 and 0.048 mA/cm^2 or 0.26 mA/cm^2 for the synthesized electrocatalysts Pt-Co/C_{AB}-DMSO, Pt-Co/C_{AB}-DMF, Pt-Co/C_{AB}-EG and Pt-Co/C_{AB}-W, respectively. In half-cell study, oxygen transport from the bulk electrolyte to the electrocatalyst may get hindered due to slow diffusion mass transfer in the liquid electrolyte solution. Moreover, the solubility of oxygen in electrolyte solution might be less. Thus, a low rate of oxygen transport to the Pt-Co/C_{AB}-EG electrocatalyst sites might result in slow ORR kinetics followed by low current density. The ORR peak at the more positive potential of 1.32 V and 1.25 V for the synthesized Pt-Co/C_{AB}-W and Pt-Co/C_{AB}-EG electrocatalyst indicates the low overpotential occurs during the cathode reduction. Whereas, the peak potentials for the other two synthesized electrocatalyst i.e., Pt-Co/C_{AB}-DMSO and Pt-Co/C_{AB}-DMF were found to be shifted towards less positive potential. Thus, these CV study results are in the similar line of all physical characterizations EDX, XRD and TEM where Pt-Co/C_{AB}-EG is expected to exhibit an excellent electrocatalytic role for ORR over the other three electrocatalysts Pt-Co/C_{AB}-DMSO, Pt-Co/C_{AB}-DMF and Pt-Co/C_{AB}-W.

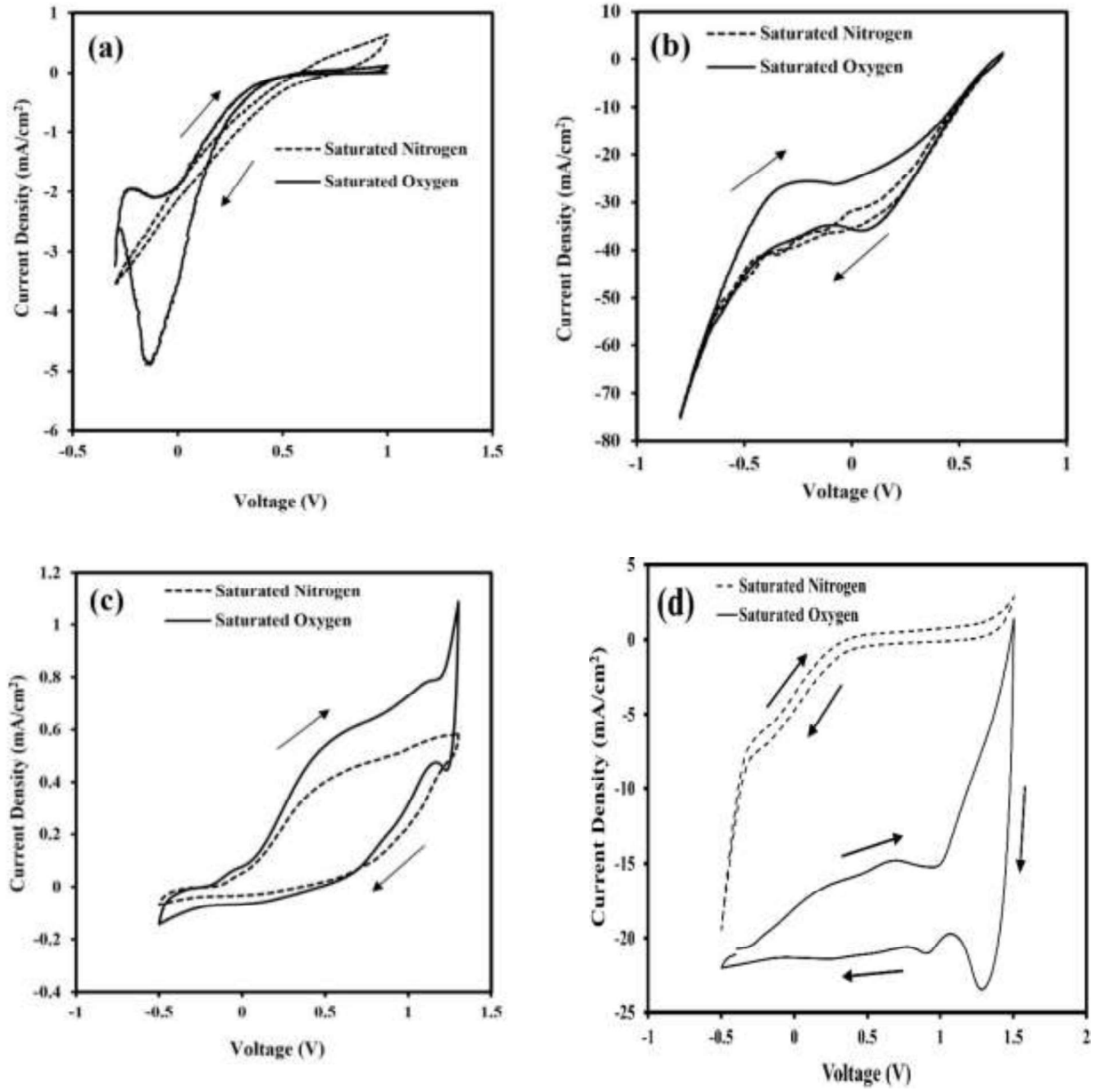

Figure 5.6 Cyclic voltammetry for synthesized electrocatalyst (a) Pt-Co/C_{AB}-DMSO, (b) Pt-Co/C_{AB}-DMF, (c) Pt-Co/C_{AB}-EG and (d) Pt-Co/C_{AB}-W of fixed loading 1 mg/cm^2 at 100 mV/s scan rate using 0.5 M $HClO_4$ electrolyte saturated with nitrogen or oxygen.

5.1.2.2 Electrochemical impedance spectroscopy (EIS) analysis

The EIS analysis of the three synthesized electrocatalysts Pt-Co/C_{AB}-DMSO, Pt-Co/C_{AB}-DMF and Pt-Co/C_{AB}-EG were performed in oxygen saturated solution mixed with 0.5 M $HClO_4$ using

frequency ranges from 100 mHz to 100 kHz at the applied voltage of 0.85 V (vs Ag/AgCl). The charge transfer resistance of electrolyte indicates the ability to conduct the ions during fuel cell operation. It is seen from Figure 5.7a that the arc radius of semi circles get reduced in the order of Pt-Co/C_{AB}-DMSO > Pt-Co/C_{AB}-DMF > Pt-Co/C_{AB}-EG, when the type of cathode electrocatalysts was varied for EIS study. It may be due to the exponential decrease in the interfacial charge transfer resistance (R_2) of varying electrode conductivity of the synthesized electrocatalysts as shown in the equivalent circuit diagram correspond to EIS (Figure 5.7b) (Panjiara and Pramanik 2021). The smaller arc radius indicates lower charge transfer resistance of the synthesized electrocatalyst (Singh et al., 2015; Lee et al., 2019 and Sun et al., 2014). Thus, it may be concluded from Figure 5.7a that the charge transfer resistance of Pt-Co/C_{AB}-EG electrocatalyst is lowest as compared to Pt-Co/C_{AB}-DMSO and Pt-Co/C_{AB}-DMF electrocatalyst.

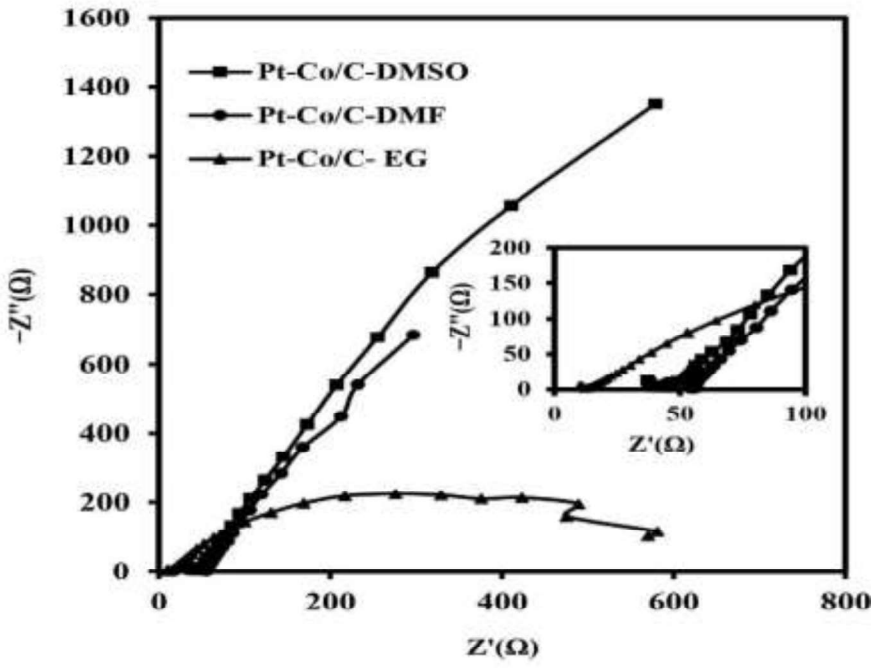

Figure 5.7a Nyquist plot of synthesized cathode electrocatalysts Pt-Co/C_{AB}-DMSO, Pt-Co/C_{AB}-DMF, and Pt-Co/C_{AB}-EG at 0.85 V in oxygen saturated 0.5 M $HClO_4$; Temperature 30 ^oC.

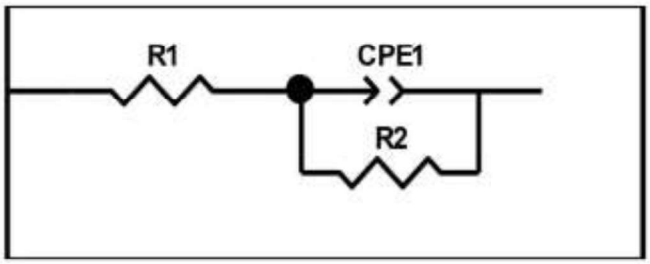

Figure 5.7b Equivalent circuit diagram corresponds to the Nyquist plot obtained from EIS.

The equivalent circuit (EC) obtained from the Nyquist plot (Figure (7a)) is presented in Figure 5.7b. In order to analyze the electronic properties of the Pt-Co/C_{AB}-DMSO, Pt-Co/C_{AB}-DMF and Pt-Co/C_{AB}-EG electrocatalysts, the Z-view software (version 3.4e, AMETEK, USA) was used to obtain the quantitative information from the EC. In the EC, a series combination of solution resistance ($R_{1)}$ and charge transfer ($R_{2)}$ in parallel with the constant CPE_1 are presented. Where CPE_1 is associated with a constant phase element which represents a double layer capacitance. It comes from electrode roughness, surface homogeneity, and porosity (Ruiz-Camacho et al., 2017). It is clearly observed from Table 5.5 that the electrocatalyst Pt-Co/C_{AB}-EG offers the lowest charge transfer resistance (R_2) of 724 Ω, solution resistance (R_1) of 12.57 Ω and double layer capacitance (CPE_1) of 0.75 mF as compared to synthesized electrocatalysts Pt-Co/C_{AB}-DMF and Pt-Co/C_{AB}-DMF, respectively. The lowest charge transfer resistance (724 Ω) of Pt-Co/C_{AB}-EG may be due to the high degree of alloying (26.36 %) as presented in the XRD analysis (Table 5.1, Page no. 64).

Table 5.5 Performance parameters of equivalent circuit obtained from Z-view software.

Electrocatalyst Type	**R_1 (Ω)**	**CPE_1 (mF)**	**R_2 (Ω)**
Pt-Co/C_{AB}-DMSO	42.95	1.10	10×10^{19}
Pt-Co/C_{AB}-DMF	55.15	1.89	4313
Pt-Co/C_{AB}-EG	12.57	0.75	724

5.1.3 Performance study of synthesized Pt-Co(3:1)/C_{AB} electrocatalyst in single cell PEMFC

5.1.3.1 Comparative performance of cathode electrocatalyst

The electrocatalytic activity of the synthesized Pt-Co/C_{AB}-DMSO, Pt-Co/C_{AB}-DMF, Pt-Co/C_{AB}-EG and Pt-Co/C_{AB}-W cathode with Pt to Co (3:1) atomic ratio electrocatalysts were investigated in a single cell setup of PEMFC (Figure 5.8). The electrocatalyst loading at the anode was 1 mg/cm^2 of commercial electrocatalyst Pt/C_{HSA}. The cathode was made of synthesized electrocatalyst Pt-Co/C_{AB}-DMSO or Pt-Co/C_{AB}-DMF or Pt-Co/C_{AB}-EG or Pt-Co/C_{AB}-W of fixed loading 1 mg/cm^2 for each set of experiments. The effective flow channel area for fuel hydrogen and oxidant oxygen was maintained at 6.25 cm^2 (2.5 cm x 2.5 cm). The PEMFC was operated at a room temperature of 33 ^oC to find out the best cathode electrocatalyst in terms of cell performance. It is seen from the Figure 5.8 that the electrocatalyst Pt-Co/C_{AB}-EG resulted in noticeably improved cell performance in comparison to the electrocatalyst Pt-Co/C_{AB}-DMSO and Pt-Co/C_{AB}-DMF. The maximum open circuit voltage (OCV) of 0.896 V was obtained for Pt-Co/C_{AB}-EG, which is a little higher in comparison to that of electrocatalyst Pt-Co/C_{AB}-DMSO, Pt-Co/C_{AB}-DMF and Pt-Co/C_{AB}-W (Table 5.6). The PEMFC constructed with Pt-Co/C_{AB}-EG cathode electrocatalyst yielded a maximum power density of 19.46 mW/cm^2 at a current density of 51.20 mA/cm^2, which is higher than those with synthesized Pt-Co/C_{AB}-DMSO (8.06 mW/cm^2), Pt-Co/C_{AB}-DMF (8.39 mW/cm^2) and Pt-Co/C_{AB}-W (7.97 mW/cm^2) cathode electrocatalysts (Table 5.6). The maximum power density increased to more than double when synthesized cathode Pt-Co/C_{AB}-EG was used in place of the other two synthesized cathode electrocatalysts Pt-Co/C_{AB}-DMSO or Pt-Co/C_{AB}-DMF or Pt-Co/C_{AB}-W at the same operating conditions. All electrocatalysts experienced a rapid drop in cell voltage, which can be attributed to the slow ORR at the cathode electrode surface during the startup of the cell reaction. This is also known as activation loss. It is

clearly seen in the Figure 5.8 that the activation loss reduces significantly when current density of more than 6.4 mA/cm^2 is drawn from the PEMFC made of Pt-Co/C_{AB}-EG cathode.

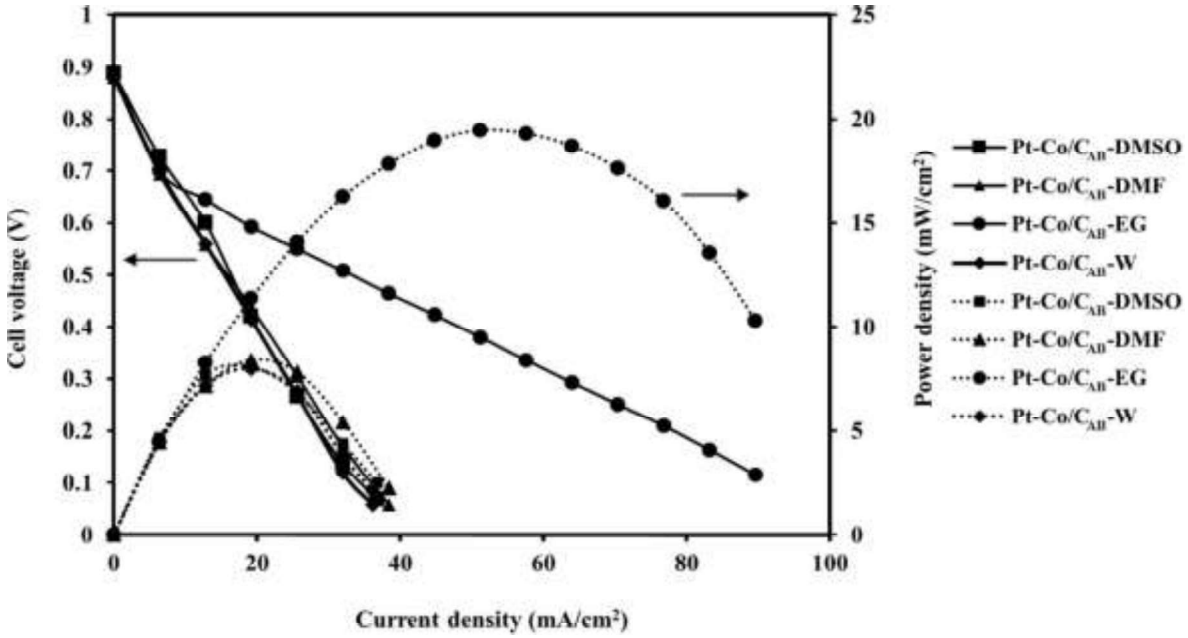

Figure 5.8 Polarization and power density curves for commercial anode Pt/C_{HSA} electrocatalyst of loading 1 mg/cm^2 and synthesized cathode Pt-Co/C_{AB}-DMSO, Pt-Co/C_{AB}-DMF, Pt-Co/C_{AB}-EG and Pt-Co/C_{AB}-W electrocatalysts of loading 1 mg/cm^2 respectively, in proton exchange membrane fuel cell at the operating temperature of 33 ºC; Dotted line – power density curves; Solid lines – polarization curves.

Table 5.6 Summary of performance of synthesized Pt-Co/C_{AB}-DMSO, Pt-Co/C_{AB}-DMF, Pt-Co/C_{AB}-EG and Pt-Co/C_{AB}-W cathode electrocatalysts in proton exchange membrane fuel cell at a room temperature of 33 ºC.

Electrocatalyst Type	OCV (V)	Maximum power density (mw/cm^2)	Current density at a maximum power density (mA/cm^2)
Pt-Co/C_{AB}-DMSO	0.888	8.06	19.2
Pt-Co/C_{AB}-DMF	0.880	8.39	19.2
Pt-Co/C_{AB}-EG	0.896	19.46	51.2
Pt-Co/C_{AB}-W	0.881	7.97	19.2

It helps to maintain higher operational cell voltage, which intern gives better cell performance in terms of power density. Whereas, activation loss was found to be very high for the Pt-Co/C_{AB}-DMSO and Pt-Co/C_{AB}-DMF when the current (i) > 0 is drawn from the cell. The lower activation overpotential was also observed in the CV study of Pt-Co/C_{AB}-EG (Figure 5.6c). The ohmic loss was found to be low for the Pt-Co/C_{AB}-EG cathode which has already shown the lowest charge transfer resistance of 724 Ω in the EIS study (Table 5.5; Figure (5.7(a-b)). Another reason for the excellent performance of Pt-Co/C_{AB}-EG may be due to the highest degree of alloying of Co i.e., 26.36 % in the Pt-Co alloy than that of Pt-Co/C_{AB}-DMSO (3.26 %), Pt-Co/C_{AB}-DMF (8.97 %) and Pt-Co/C_{AB}-W (0.27 %) electrocatalysts (Table 5.1, Page no. 64) (Salgado et al., 2004; Santiago et al., 2007 and Jayasayee et al., 2012). The electrocatalyst synthesized using different solvent (DMSO or DMF or EG or W) in atomic ratio of 1:1 and 1:3 also gives poor performance as compare to Pt-Co(3:1)/C_{AB}-EG. The characteristics of polarization and power density curves are presented in Appendix D (Figure D1 to Figure D2). It is clear from the performance comparison of four cathode electrocatalysts that Pt-Co/C_{AB}-EG cathode comes up with several good properties which are found due to some special characteristics of the solvent ethylene glycol (EG). The ethylene glycol reduces a metal precursor directly to metallic platinum (Aoun et al., 2016). Ethylene glycol scavenges hydroxyl radicals like 2-propanol, resulting in the production of reactive radicals with reducing characteristics (Esmaeilifar et al., 2010). Due to this reducing ability, the ethylene glycol is employed as a reducing agent and solvent in the preparation of high-activity core-shell electrocatalysts, allowing for fine control of particle shape and size.

5.1.3.2 Effect of anode loading

The polarization and power density curves for the varying anode loading ranging from 0.75 to 1.25 mg/cm^2 of commercial Pt/C_{HSA} and the fixed cathode loading of 1 mg/cm^2 Pt-Co(3:1)/C_{AB}-EG are

presented in the Figure 5.9. As the synthesized Pt-Co/C_{AB}-EG exhibited the highest cell performance in terms of power density and thus, it was selected as a cathode electrocatalyst for the optimization of anode loading. It is seen from the Figure 5.9 that the polarization and power density curves shifted upward with the increase in anode loading from 0.75 mg/cm^2 to 1 mg/cm^2 and further increase in anode loading to 1.25 mg/cm^2, the curves shifted downward. The Figure 5.9 shows that the highest cell performance in terms of power density i.e., 19.56 mW/cm^2 was obtained for the optimum anode loading of 1 mg/cm^2. Whereas, the highest anode loading of 1.25 mg/cm^2 resulted in a lower power density (14.8 mW/cm^2) than that of 1 mg/cm^2 anode loading. It may be due to agglomeration of the anode electrocatalyst at a very high loading of 1.25 mg/cm^2 within the anode electrode structure, the active sites of the electrocatalyst get decreased (Panjiara and Pramanik 2022).

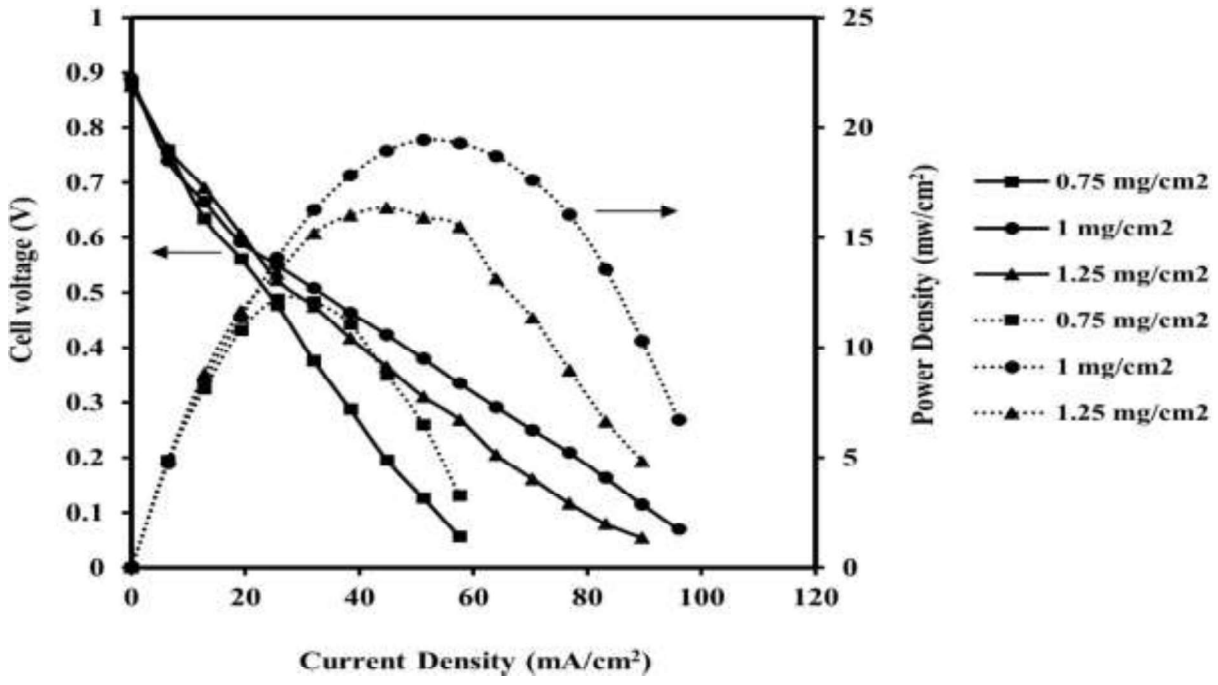

Figure 5.9 Polarization and power density curves for varying loading of commercial anode Pt/C_{HSA} electrocatalyst and fixed loading of 1 mg/cm^2 synthesized Pt-Co/C_{AB}-EG cathode electrocatalyst in proton exchange membrane fuel cell at an operating temperature of 33 ºC; Dotted line – power density curves; Solid lines – polarization curves.

Thus, the interaction between fuel gas H_2 and electrocatalyst also decreases. This resulted in a low power density at a very high anode loading of 1.25 mg/cm^2. In addition, the porosity of the anode electrocatalyst layer decreases when the number of electrocatalyst particles were increased within the same area of the anode electrode i.e., 2.5 cm x 2.5 cm. Due to the low porosity of the anode, mass transfer from the bulk phase to the electrocatalyst layer decreases significantly, and thereby, the power density obtained was low. However, the anode loading of 1 mg/cm^2 Pt/C_{HSA} resulted in the highest power density and it may be due to the uniform distribution of the anode electrocatalyst without any agglomeration (Rathoure and Pramanik 2016).

5.1.3.3 Effect of cathode loading

5.1.3.3.1 Pt-Co(3:1)/C_{AB}-EG as cathode electrocatalyst

Figure 5.10 shows the polarization and power density curves for different cathode loading varying from 0.75 to 1.25 mg/cm^2 of Pt-Co/C_{AB}-EG and optimum anode electrocatalyst loading of 1 mg/cm^2 which was kept fixed at the anode. It is clearly seen from the Figure 5.10 that the current density and power density both increase with the increase in cathode electrocatalyst loading from 0.75 to 1 mg/cm^2. The PEMFC gives poor performance in terms of current density and power density when the cathode loading was increased beyond 1 mg/cm^2. Similar trends were observed here also (Figure 5.10), as it was seen in the case of anode loading (Figure 5.9). The reason for such a trend of PEMFC characteristics with electrocatalyst loading has already been discussed earlier in the section 5.1.3.2 Effect of anode loading. The highest power density of 19.46 mW/cm^2 at a current density of 51.2 mA/cm^2 was obtained for the optimum cathode loading of 1 mg/cm^2 Pt-Co/C_{AB}-EG. Whereas, maximum power density of 9.77 mW/cm^2 and 11.55 mW/cm^2 were obtained at the current density of 22.4 mA/cm^2 and 32 mA/cm^2 for the cathode loading of 0.75 mg/cm^2 and 1.25 mg/cm^2, respectively.

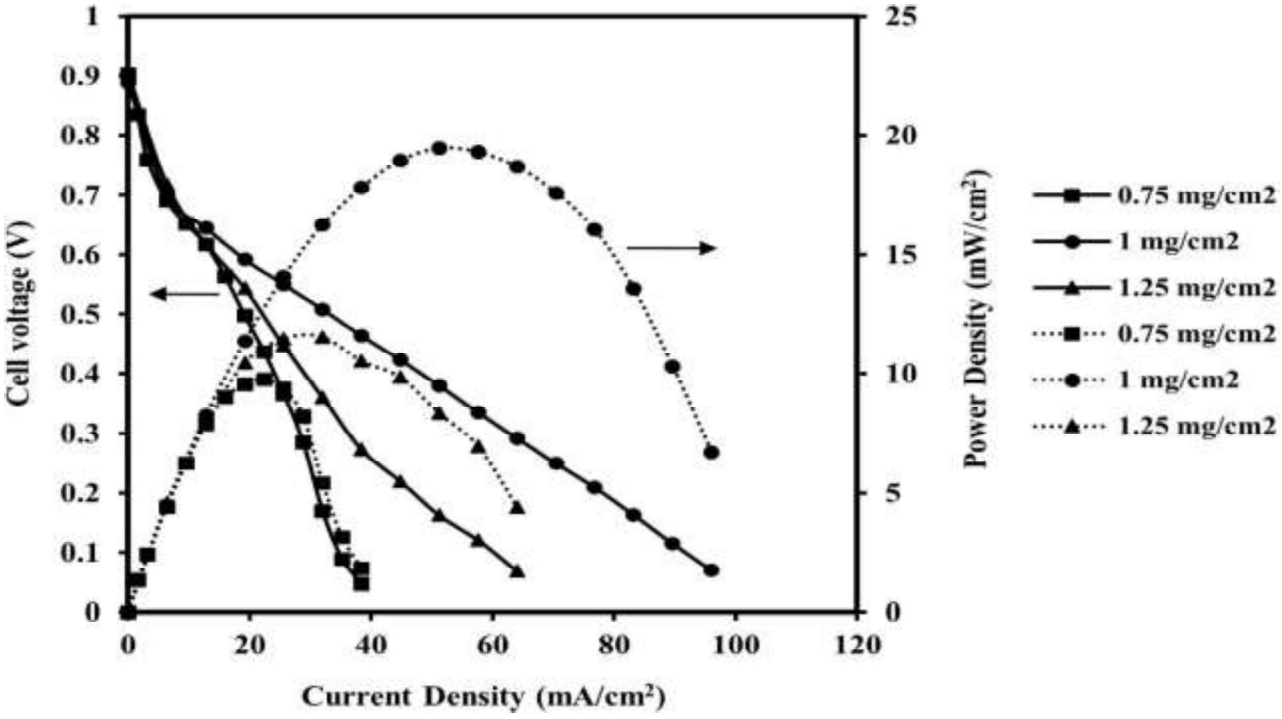

Figure 5.10 Polarization and power density curves for commercial anode Pt/C_{HSA} of fixed optimum loading of 1 mg/cm^2 and synthesized Pt-Co/C_{AB}-EG cathode electrocatalyst of varying loading in proton exchange membrane fuel cell at an operating temperature of 33 ^oC; Dotted line – power density curves; Solid lines – polarization curves.

5.1.3.3.2 Pt-Co(3:1)/C_{AB}-DMF as cathode electrocatalyst

Figure 5.11 shows the polarization curves and power density curves for different cathode loading varying from 0.75 mg/cm^2 to 1.25 mg/cm^2 of Pt-Co/C_{AB}-DMF, with a fixed and optimum anode loading of 1 mg/cm^2 Pt/C_{HSA}. It is seen in Figure 5.11 that the synthesized cathode electrocatalyst Pt-Co/C_{AB}-DMF loading of 1 mg/cm^2 produced the highest power density of 8.39 mW/cm^2 at a current density of 19.20 mA/cm^2. The highest power density (8.39 mW/cm^2) produced here for the cathode electrocatalyst Pt-Co/C_{AB}-DMF was lower in comparison to that of cathode electrocatalyst Pt-Co/C_{AB}-EG (19.56 mW/cm^2). The electrocatalyst Pt-Co/C_{AB}-DMF loading of 0.75 mg/cm^2 and 1.25 mg/cm^2 produced low power density of 5.09 mW/cm^2 and 7.56 mW/cm^2,

respectively. The trend of polarization and power density curves with cathode electrocatalyst loading for Pt-Co/C_{AB}-DMF were similar to that of Pt-Co/C_{AB}-EG cathode electrocatalyst (Figure 5.10). The power density decreased to 7.56 mW/cm^2 with an increase in cathode loading to 1.25 mg/cm^2. The reason for this decrease may be electrocatalyst agglomeration. The electrocatalyst agglomeration results in a decrease in porosity of the electrocatalyst layer leading to increased diffusional resistance to flow transport of oxygen from the flow channel to the cathode electrocatalyst zone.

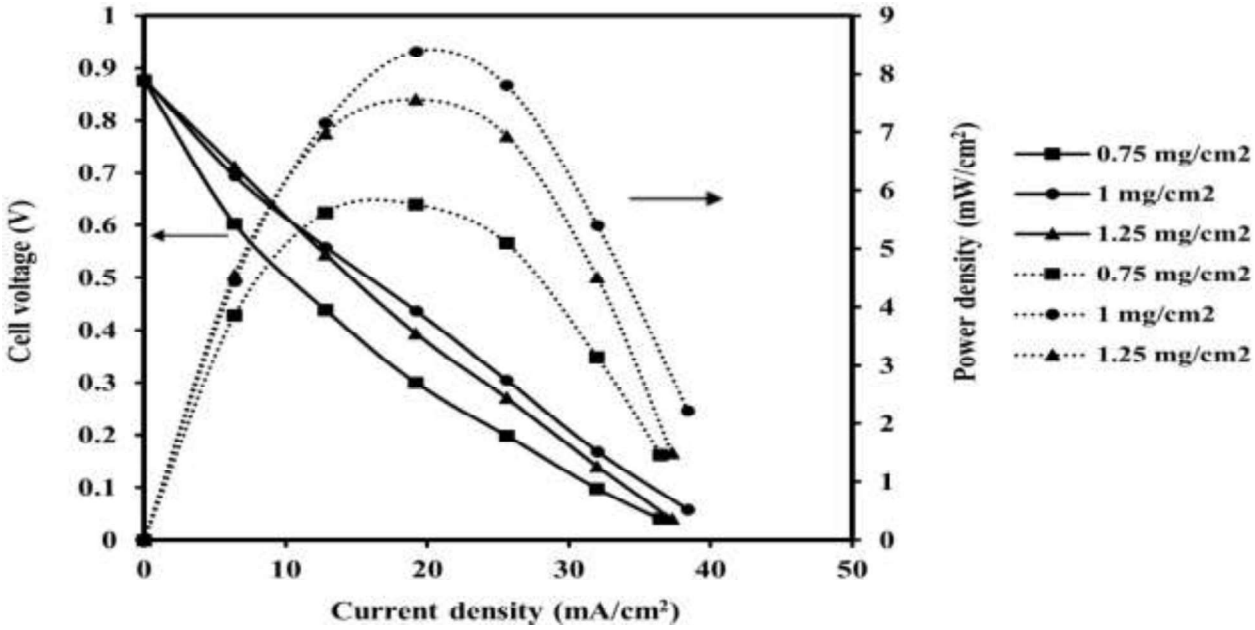

Figure 5.11 Polarization and power density curves for commercial anode Pt/C_{HSA} of fixed optimum loading of 1 mg/cm^2 and synthesized Pt-Co/C_{AB}-DMF cathode electrocatalyst of varying loading in proton exchange membrane fuel cell at an operating temperature of 33 ^oC; Dotted line – power density curves; Solid lines – polarization curves.

5.1.3.3.3 Pt-Co(3:1)/C_{AB}-DMSO as cathode electrocatalyst

The polarization and power density curves are shown in Figure 5.12 for cathode Pt-Co/C_{AB}-EG loadings ranging from 0.75 to 1.25 mg/cm^2 and the anode electrocatalyst Pt/C_{HSA} fixed loading of 1 mg/cm^2. The maximum power density obtained was 8.06 mW/cm^2 at a current density of 19.20

mA/cm^2 for the optimum cathode loading of 1 mg/cm^2 Pt-Co/C_{AB}-DMSO. The cell performance decreased to 6.89 mW/cm^2 upon increasing the cathode loading to 1.25 mg/cm^2. The highest power density (8.06 mW/cm^2) produced at optimum cathode loading for Pt-Co/C_{AB}-DMSO was lower than cathodes Pt-Co/C_{AB}-EG (19.56 mW/cm^2) and Pt-Co/C_{AB}-DMF (8.39 mW/cm^2) at their optimum loading of 1 mg/cm^2, respectively.

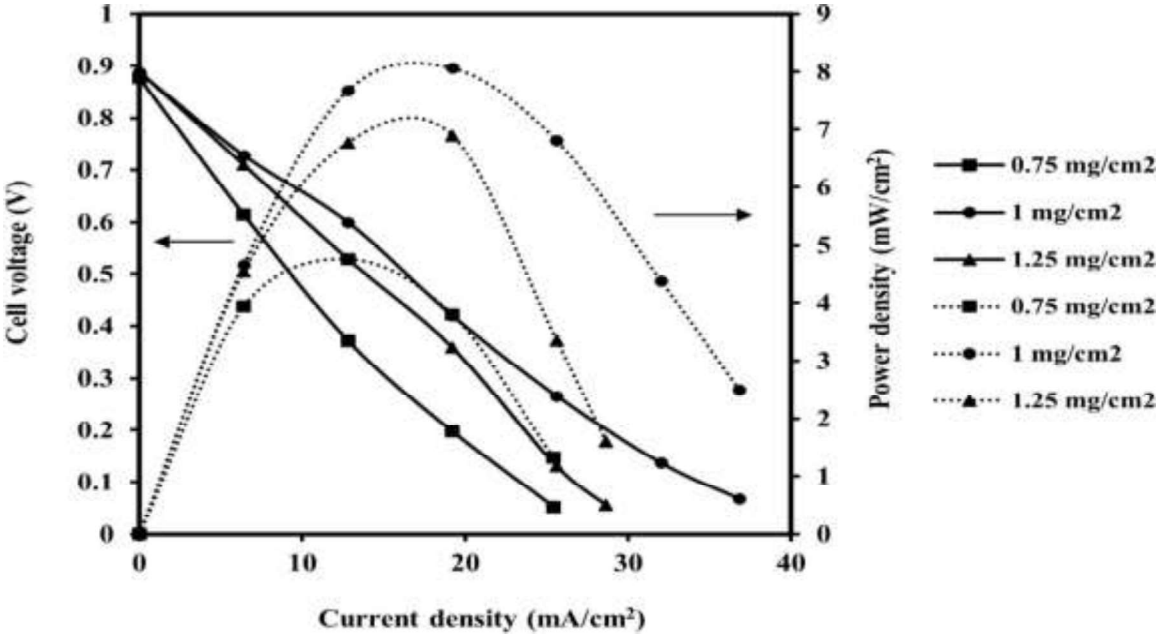

Figure 5.12 Polarization and power density curves for commercial anode Pt/C_{HSA} of fixed optimum loading of 1 mg/cm^{2}and synthesized Pt-Co/C_{AB}-DMSO cathode electrocatalyst of varying loading in proton exchange membrane fuel cell at operating cell temperature of 33 ºC; Dotted line – power density curves; Solid lines – polarization curves.

5.1.3.3.4 Pt-Co(3:1)/C_{AB}-W as cathode electrocatalyst

The identical results were obtained when the Pt-Co/C_{AB}-W cathode electrocatalyst loading was changed from 0.75 mg/cm^2 to 1.25 mg/cm^2, keeping the anode loading fixed at 1 mg/cm^2 Pt/C_{HSA} (Figure 5.13). At optimum cathode loading of 1 mg/cm^2 Pt-Co/C_{AB}-W, the maximum power density of 7.97 mW/cm^2 was obtained at a current density of 19.20 mA/cm^2. When the cathode loading was increased to 1.25 mg/cm^2, the cell performance dropped to 7.49 mW/cm^2. It should

be noted that the maximum power density (7.97 mW/cm^2) obtained by Pt-Co/C_{AB}-W at optimum cathode loading was lower than the other three cathodes, Pt-Co/C_{AB}-EG (19.56 mW/cm^2), Pt-Co/C_{AB}-DMF (8.39 mW/cm^2) and Co/C_{AB}-DMSO (8.06 mW/cm^2) at their optimum loading of 1 mg/cm^2. This reduction in power density may be caused by electrocatalyst agglomeration, which reduces the available porosity of the electrocatalyst layer for flowing the oxygen. It is already discussed in the previous section.

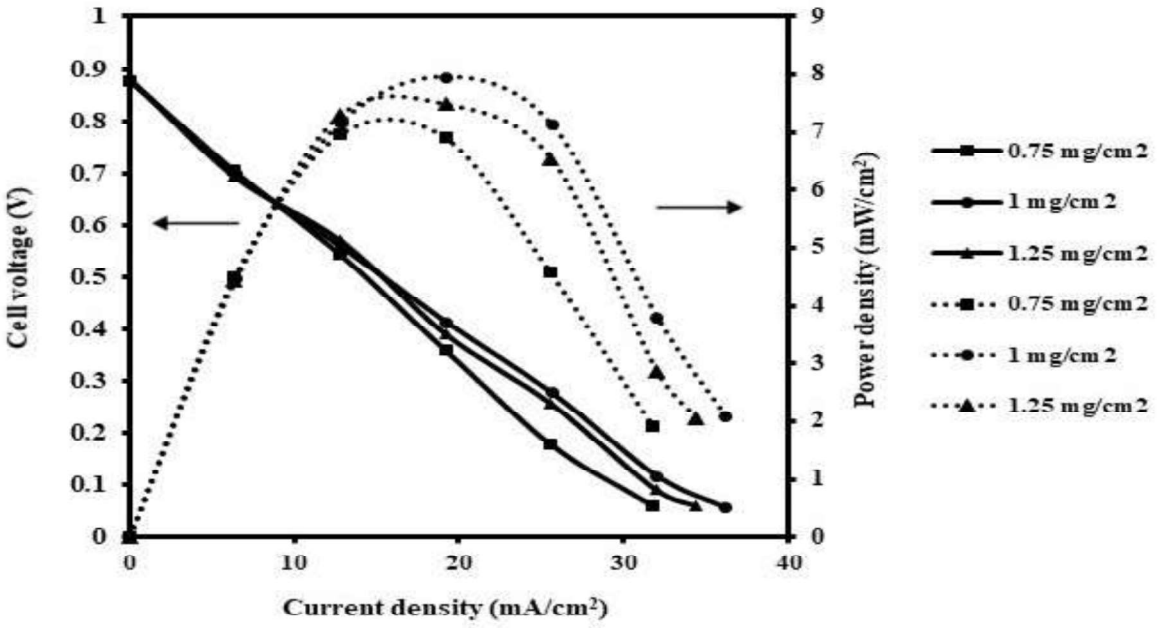

Figure 5.13 Polarization and power density curves for commercial anode Pt/C_{HSA} of fixed optimum loading of 1 mg/cm^{2}and synthesized Pt-Co/C_{AB}-W cathode electrocatalyst of varying loading in proton exchange membrane fuel cell at operating cell temperature of 33 ^oC; Dotted line – power density curves; Solid lines – polarization curves.

5.1.3.4 Effect of temperature in PEMFC

The best cathode electrocatalyst Pt-Co(3:1)/C_{AB}-EG was considered at cathode side for the investigation of temperature effect on the PEMFC. The optimum cathode electrocatalyst loading of 1 mg/cm^2 and anode loading of 1 mg/cm^2 (Pt/C_{HSA}) were considered. The cell temperature was

varied from room temperature i.e., 33 ºC to 80 ºC to evaluate the cell performance at high temperature. The performance characteristics i.e., polarization and power density curves at varying temperature for Pt/C_{HSA} anode and Pt-Co/C_{AB}-EG cathode electrocatalyst is shown in the Figure 5.14. It is clearly seen in the Figure 5.14 that both the curves shifted upward with the increase in temperature up to 70 ºC and after that cell performance decreases when the temperature is increased to 80 ºC. The temperature of PEMFC was not increased further keeping in mind the dehydration of PEM electrolyte and electrode catalyst layer. The enhancement in performance of PEMFC with the increase in temperature was due to faster reaction kinetics at anode and cathode, respectively. Moreover, at the higher temperature, electronic conductivity and mobility of electrons improve and thus, ohmic resistance decreases in PEMFC which further enhanced the cell performance as compared to lower temperature (Askaripour, 2019). However, open circuit voltage/OCV got reduced when the temperature was increased from 33 ºC to 80 ºC successively. The Nernst equation could be used to explain the temperature dependence of OCV. The maximum OCV of 0.896 V was obtained at a temperature of 33 ºC. Whereas, little low OCV of 0.886 V was recorded at the elevated temperature of 80 ºC (Table 5.7). The maximum power density of 26.11 mW/cm^2 at a current density 76.8 mW/cm^2 was obtained at the highest cell operation temperature of 70 ºC. On the other side at room temperature of 33 ºC, the PEMFC resulted in maximum power density of 19.61 mW/cm^2 at a current density of 51.20 mA/cm^2 which is lower than that of the power density obtained at 70 ºC.

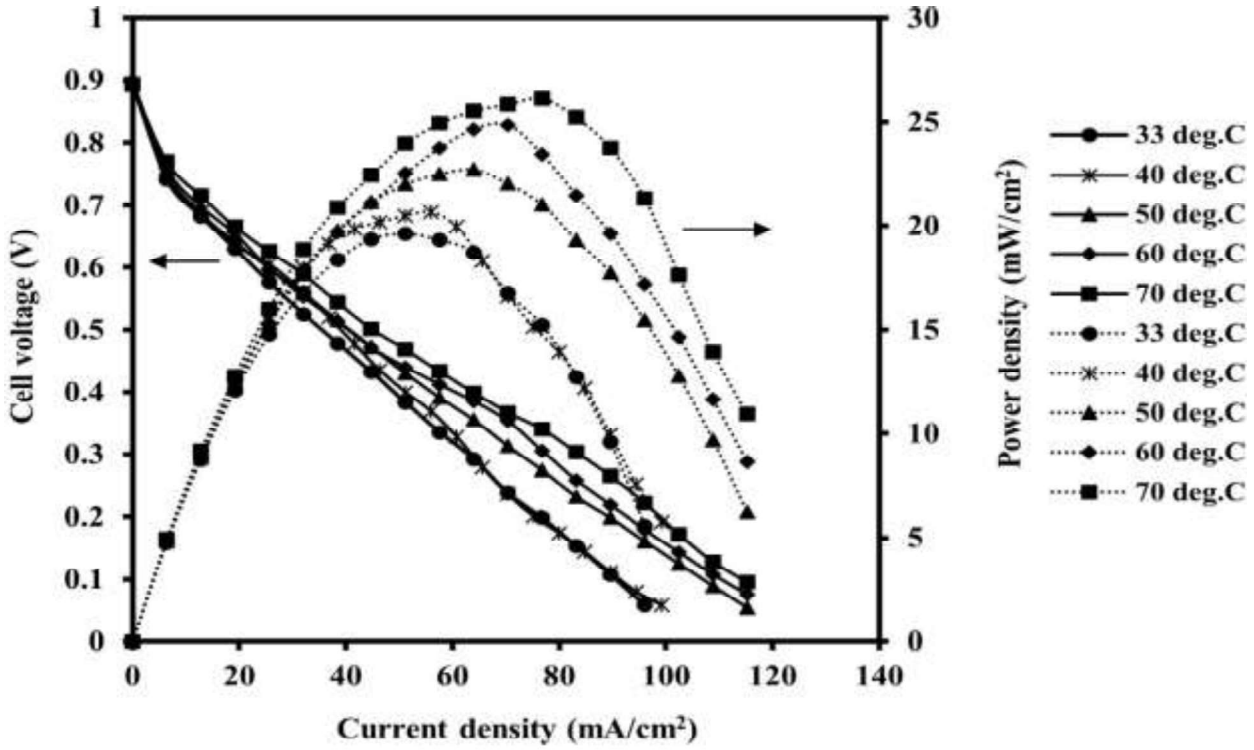

Figure 5.14 Polarization and power density curves for commercial anode Pt/C_{HSA} electrocatalyst and synthesized $Pt\text{-}Co/C_{AB}$-EG cathode electrocatalyst keeping fixed optimum loading of 1 mg/cm^2 at both the electrodes; Dotted line – power density curves; Solid lines – polarization curves.

Table 5.7 Summary of performance of the synthesized best cathode $Pt\text{-}Co/C_{AB}$-EG electrocatalyst using optimum loading of 1 mg/cm^2 in PEMFC at various operating temperatures.

Temperature (^oC)	OCV (V)	Maximum power density (mW/cm^2)	Current density at a maximum power density (mA/cm^2)
33	0.896	19.61	51.2
40	0.895	20.66	56
50	0.894	22.72	64
60	0.891	24.85	70.4
70	0.890	26.11	76.8
80	0.886	24.14	70.4

5.2 Pt-Ni(3:1)/C_{AB} cathode electrocatalyst performance evaluation: Part II

5.2.1 Physical characterization

5.2.1.1 X-ray diffraction (XRD) analysis

The XRD patterns of Pt-Ni/C_{AB}-DMSO, Pt-Ni/C_{AB}-DMF and Pt-Ni/C_{AB}-EG electrocatalysts with Pt to Ni 3:1 atomic ratio are shown in Figure 5.15. The XRD diffraction confirmed the development of well-alloyed Pt-Ni/C_{AB} nano-range electrocatalyst. In all three synthesized electrocatalysts the diffraction at 2θ peak position between 25-26°, the hexagonally structured (002) plane of acetylene black carbon support was found. The XRD patterns shows also the highly crystalline face-centered cubic (FCC) structure Pt-phase in all synthesized Pt-Ni/C_{AB} electrocatalysts. The crystalline planes at 2θ about 39°, 46°, 67°, and 81°, which reflect crystalline FCC, were assigned to the crystalline planes Pt (111), (200), (220 and (311), respectively. The shifting in the higher 2θ angles of the Pt peaks for synthesized electrocatalyst Pt-Ni/C_{AB}-DMSO, Pt-Ni/C_{AB}-DMF and Pt-Ni/C_{AB}-EG are shown in Figure 5.15.

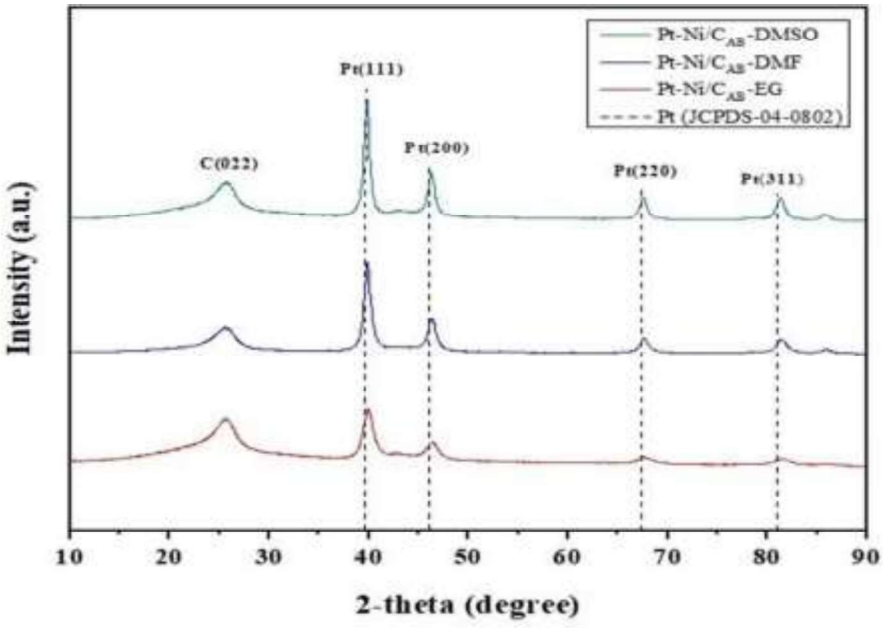

Figure 5.15 XRD patterns of synthesized electrocatalysts Pt-Ni/C_{AB}-DMSO, Pt-Ni/C_{AB}-DMF and Pt-Ni/C_{AB}-EG.

Table 5.8 Lattice parameters and the crystallographic properties at Pt (220) diffraction peak of Pt-Ni/C_{AB} synthesized electrocatalyst.

Electrocatalyst Types	2θ (°)	Crystallite size (d_c) (nm)	Alloying degree (%)
Pt-Ni/C-DMSO	67.51	11.91	6.22
Pt-Ni/C-DMF	67.51	10.46	6.22
Pt-Ni/C-EG	67.50	6.04	7.47
Pt (JCPDS 04-0802)	67.45	–	–

This shows the forming of alloys between Pt and Ni due to the incorporation of Ni into the Pt metal FCC structure (Hyun et al., 2013 and Tayal et al., 2012). Figure 5.15 also shows the clear shifting of peak for the Pt (220) plane of synthesized electrocatalyst as compared to 2θ peak position (JCPDS 04-0802) of Pt bulk (220) plane. The Pt (220) plane peak position was taken to measure the average crystallite size (d_c), lattice parameter (a), and degree of alloying, because this peak position is far from the background position of electrocatalyst support material i.e., C_{AB} (Hyun et al., 13 and Lima et al., 2006). The degree of allying was calculated using Vegard's law and using the formula given by Hyun et al., (2013) shown in Equations (5.4) to (5.5).

$$a_{(220)} = 0.38013 + 0.0124\, x_{Pt} \tag{5.4}$$

$$M_{alloy} = \frac{x_{Pt}}{(1-x_{Pt})(M/N)_{nom}} \tag{5.5}$$

Where, M_{alloy} is alloy percentage of Pt in Pt-Ni/C_{AB} metal alloy, $a_{(220)}$ is lattice parameter of synthesized Pt-Ni/C_{AB} metal alloy at Pt (220) plane position, x_{Pt} is platinum atomic fraction in Pt-Ni/C_{AB} metal alloy, and $(M/N)_{nom}$ is nominal atomic ratio of Pt and Ni.

The atomic fraction of Pt (x_{Pt}) was calculated using lattice parameter of Pt-Ni/C_{AB} synthesized electrocatalyst. The alloying degree of Pt was determined by using nominal atomic ratio of Pt to Ni. The lattice parameter of Pt-Ni/C_{AB}-EG metal alloy was 0.3920 nm against the pure metal Pt of 0.3924 nm (Choudhary and Pramanik 2020a). However, the lattice parameter of Pt-N/C_{AB}-DMSO and Pt-Ni/C_{AB}-DMF metal alloys were 0.3919 nm each. The average crystallite size (d_c) was determined using Scherrer's formula (Equation 5.1). The crystallite size of Pt-Ni/C_{AB}-DMSO, Pt-Ni/C_{AB}-DMF and Pt-Ni/C_{AB}-EG metal alloys were found 11.91 nm, 10.46 nm and 6.04 nm, respectively (Table 5.8). The Bragg's law (Equation 5.2) was used to calculate the d-spacing for the synthesized electrocatalysts shown as is in Table 5.8. It was predicted that the Pt-Ni/C_{AB}-EG electrocatalyst might give excellent performance in half-cell and single because the degree of alloying percentage of Pt in Pt-Ni/C_{AB}-EG is highest i.e., 7.47 wt. % as in comparison to the degree of alloying of electrocatalysts Pt-Ni(3:1)/C_{AB} (6.22 wt. %) and Pt-Ni(1:1)/C_{AB} (6.22 wt. %).

5.2.1.2. SEM-EDX analysis

The surface morphological investigation of Pt-Ni/C_{AB} synthesized electrocatalysts was seen by high resolution surface electron microscopy (HRSEM). The HRSEM images indicate that the Pt-Ni/C_{AB}-DMSO, Pt-Ni/C_{AB}-DMF and Pt-Ni/C_{AB}-EG synthesized electrocatalyst are spherical in shape and nano-range in size, as it is shown in Figure 5.16(a-c). The electrocatalyst Pt-Ni/C_{AB}-EG (Figure 5.16c) come up with more uniform surface morphology of metal alloy Pt and Ni rather than Pt-Ni/C_{AB}-DMSO (Figure 5.15a) and Pt-Ni/C_{AB}-DMF (Figure 5.16b) synthesized electrocatalysts, respectively. No agglomeration was also observed for the Pt-Ni/C_{AB}-EG. A little contrast of white spots are observed in all synthesized electrocatalyst due to coating of gold particles (Tayal et al., 2012).

The EDX was carried out to analyze the presence of carbon, oxygen, and metal particles i.e., Pt and Ni in the synthesized Pt-Ni/C_{AB} electrocatalysts. The EDX elemental spectrum of Pt-Ni/C_{AB} synthesized electrocatalyst is shown in the Figure 5.16(a-c). In the EDX, it was clearly visualized that Pt, Ni, and C are well distributed and present in the Pt-Ni/C_{AB}-DMSO, Pt-Ni/C_{AB}-DMF and Pt-Ni/C_{AB}-EG synthesized metal alloy having different ratios. The elemental composition of all desired elements is shown in Table 5.9. It was observed from the Table 5.9, that the total metal loading on the synthesized electrocatalyst is 20 wt. % that is similar to desired condition. The elemental composition of all synthesized electrocatalyst is nearly in good agreement with some variation as compare to nominal composition, which was calculated initially. However, the Pt-Ni/C_{AB} metal alloy surface is heterogeneous in nature and the elemental composition of desired elements may vary point to point in the synthesized electrocatalyst (Panjiara and Pramanik 2022; Singh and Pramanik 2022).

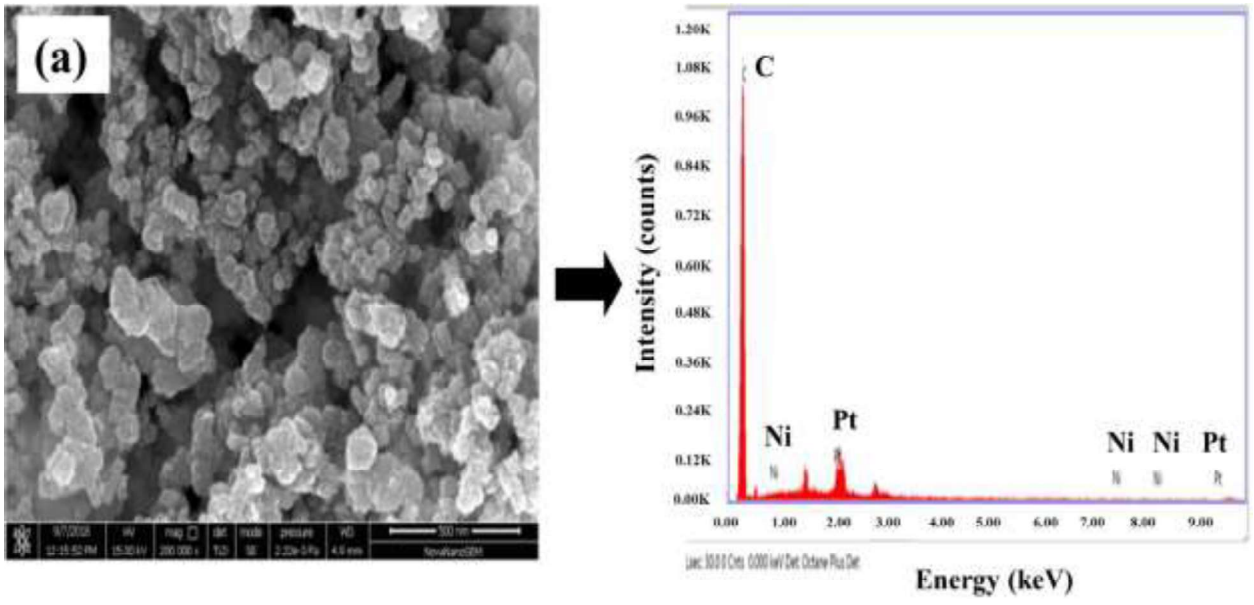

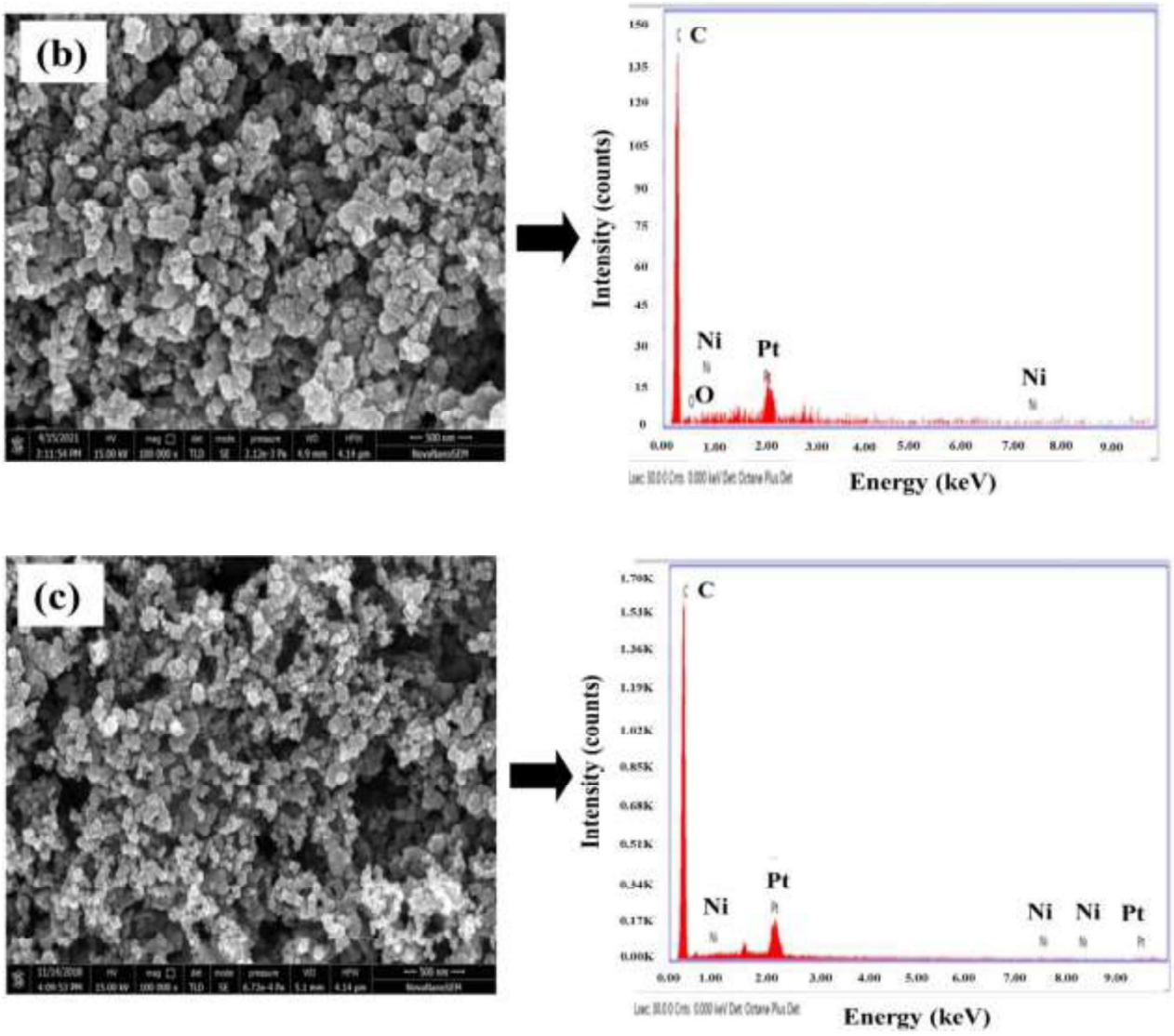

Figure 5.16 SEM/EDX images of synthesized electrocatalyst with different solvents (a) Pt-Ni/C_{AB}-DMSO, Pt-Ni/C_{AB}-DMF and Pt-Ni/C_{AB}-EG.

Table 5.9 Surface concentration of synthesized electrocatalyst obtained from EDX analysis.

Electrocatalyst type	EDX composition		Nominal composition	
	Pt (wt. %)	Ni (wt. %)	Pt (wt. %)	Ni (wt. %)
Pt-Ni/C_{AB}-DMSO	16.52	1.51	18.18	1.82
Pt-Ni/C_{AB}-DMF	16.75	1.34	18.18	1.82
Pt-Ni/C_{AB}-EG	17.01	1.42	18.18	1.82

5.2.1.3 Transmission electron microscopy (TEM) analysis

Figure 5.17(a-c) shows the TEM images and respective histograms of all synthesized Pt-Ni/C_{AB} metal alloy nanoparticles which gives the information about the particle size distribution shape, and size. The average particle size of synthesized electrocatalysts was determined by taking 75 particles from TEM image for estimation of particle size with the help of Image J software (Table 5.11). It is seen from the Figure 5.17(a-c) the dark spherical spots are scattered over acetylene black carbon support (C_{AB}) uniformly. The carbon supports were in the range of 30-50 nm as these are lighter particles. Although Pt-Ni nanoparticles i.e., dark black dots are scattered equally around the carbon support which are normally light particles in the Pt-Ni/C_{AB} synthesized electrocatalyst (Choudhary and Pramanik 2020b; Tayal et al., 2012 and Singh and Pramanik 2019). The average particle size were found for Pt-Ni/C_{AB}-DMSO of 4.54 ± 0.79 nm, Pt-Ni/C_{AB}-DMF of 3.45 ± 1.03 nm and Pt-Ni/C_{AB}-EG of 2.89 ± 0.74 nm. The particle size of Pt-Ni/C_{AB}-DMSO electrocatalyst (Figure 5.17a) has the largest particle size than other electrocatalyst Pt-Ni/C_{AB}-DMF (Figure 5.17b) and Pt-Ni/C_{AB}-EG (Figure 5.17c). Among these synthesized electrocatalysts, the Pt-Ni/C_{AB}-EG electrocatalyst has the smallest particle size of 2.89 ± 0.74 nm. The TEM average particle size (Table 5.10) and the average crystallite size observed from the XRD shows the similar trend (Table 5.8). After comparing the average particle size of the TEM and the XRD, the deference was found in particle due to special character of the XRD because the XRD reflects the crystallite size not the actual morphology of particle (Panjiara and Pramanik 2021).

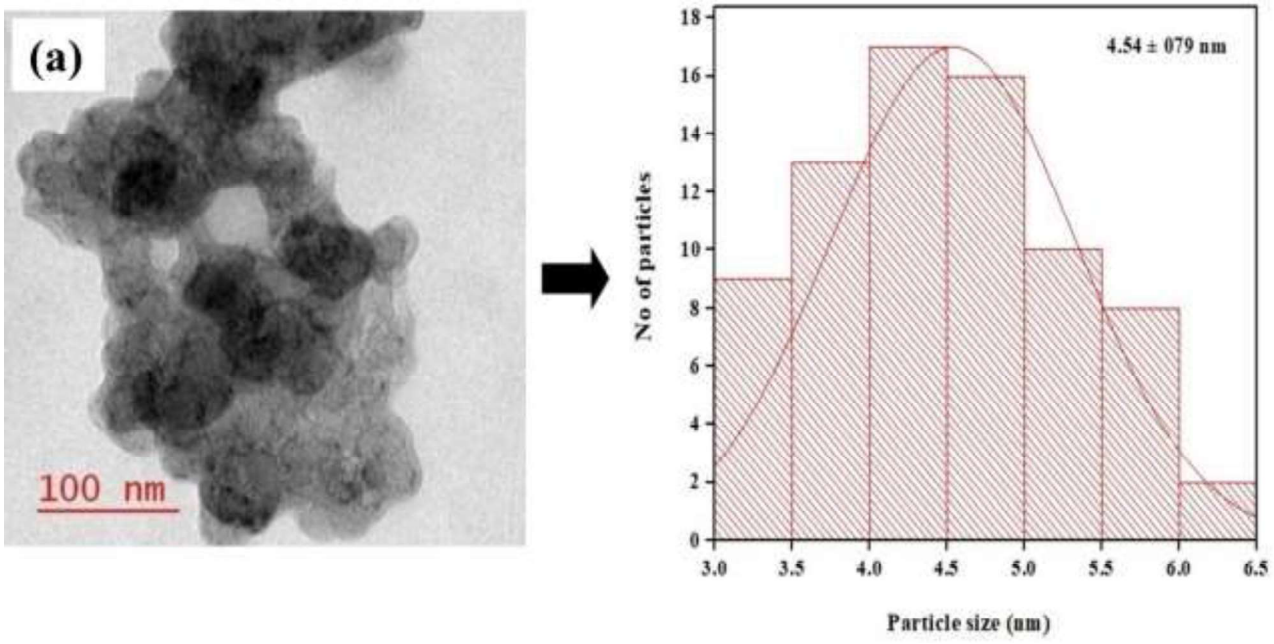
(a)
100 nm
4.54 ± 079 nm
No of particles
Particle size (nm)

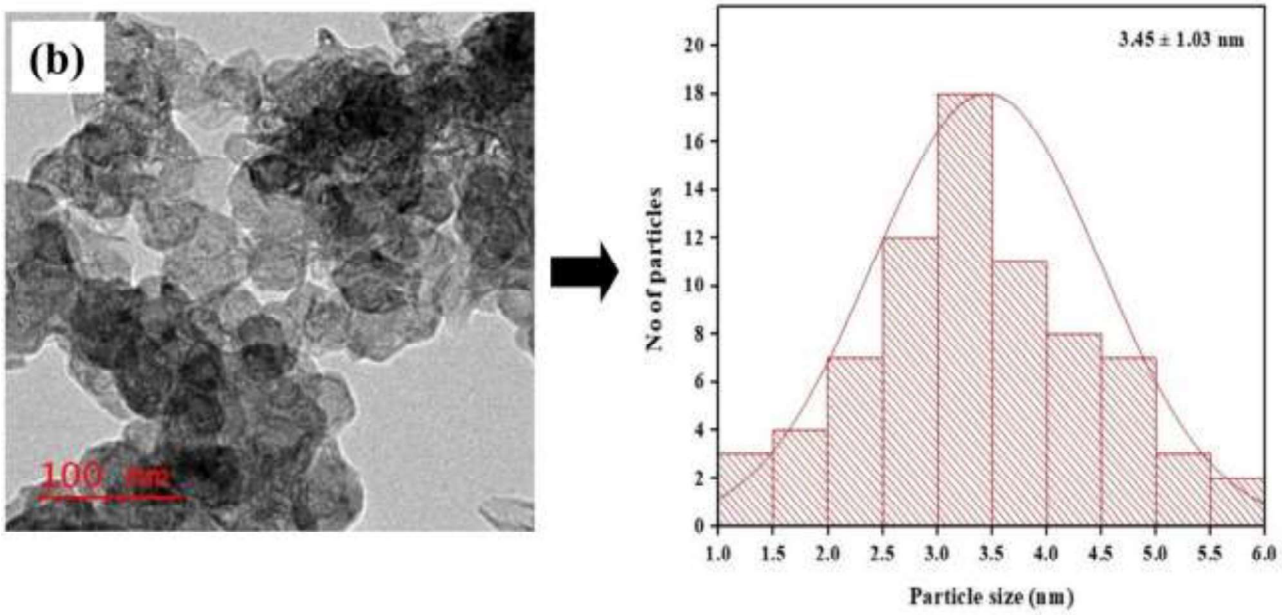
(b)
100 nm
3.45 ± 1.03 nm
No of particles
Particle size (nm)

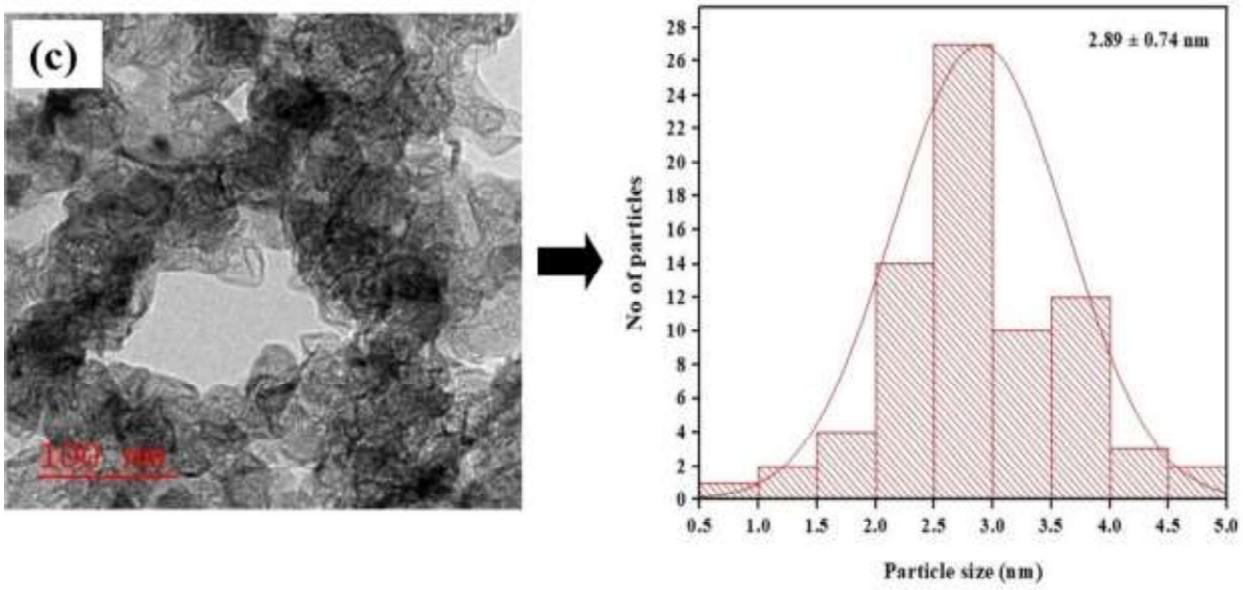

Figure 5.17 TEM images and corresponding histogram of synthesized electrocatalyst (a) Pt-Ni/C_{AB}DMSO, (b) Pt-Ni/CAB-DMF, and (c) Pt-Ni/C_{AB}-EG.

Table 5.10 The average particle size of electrocatalysts from TEM analysis and comparison with XRD average crystallite size.

Electrocatalysts	**Average particle size by TEM (nm)**	**Average particle size by XRD (nm)**
Pt-Ni/C_{AB}-DMSO	4.54 ± 0.79	11.91
Pt-Ni/C_{AB}-DMF	3.45 ± 1.03	10.40
Pt-Ni/C_{AB}-EG	2.89 ± 0.74	6.04

Table 5.11 Particle size distribution of synthesized all three Pt-Ni/C_{AB} electrocatalysts by TEM analysis.

Type of electrocatalyst	**% of particles**	**Particle size (nm)**	**No. of particles**
Pt-Ni/C_{AB}-DMSO	12	3-3.5	9
	17.33	3.5-4	13
	22.67	**4-4.5**	**17**
	21.33	4.5-5	16

Type of electrocatalyst	% of particles	Particle size (nm)	No. of particles
	13.33	5-5.5	10
Pt-Ni/C_{AB}-DMSO	10.67	5.5-6	8
	2.67	6-6.5	2
	4	1-1.5	3
	5.33	1.5-2.0	4
	9.33	2.0-2.5	7
	16	2.5-3.0	12
Pt-Ni/C_{AB}-DMF	**24**	**3.0-3.5**	**18**
	14.67	3.5-4.0	11
	10.67	4.0-4.5	8
	9.33	4.5-5.0	7
	4	5.0-5.5	3
	2.67	5.5-6.0	2
	1.33	0.5-1.0	1
	2.67	1.0-1.5	2
	5.33	1.5-2.0	4
	18.67	2.0-2.5	14
Pt-Ni/C_{AB}-EG	**36**	**2.5-3.0**	**27**
	13.33	3.0-3.5	10
	16	3.5-4.0	12
	4	4.0-4.5	3
	2.67	4.5-5.0	2

5.2.2 Electrochemical characterization of electrocatalyst

5.2.2.1 Cyclic voltammetry (CV) analysis

The electro-chemical reaction process for oxygen reduction reaction (ORR) at cathode is very complicated and requires a number of intermediates, mostly depending on electronic property of electrode, electrocatalyst and electrolyte (Yeager, 1986 and Bard et al., 1980). As already discussed in the previous section 5.1.2.1(Page no. 75), in the acidic medium oxygen reduction reaction usually takes place through either two stage 2 + 2 electron pathway chapter 1 (Equation 1.4 to Equation 1.7) or single stage 4 electron pathway (Equation 1.8). Thus, water is only byproduct at the cathode, formed by oxygen reduction reaction. The first step of the mechanism of ORR is the chemisorption of oxygen molecules on the Pt surface and then subsequently, oxygen removal chapter 1 (Equation 1.4). The peaks of oxygen reduction were found in the reverse CV scan. The size of the reverse scan oxygen reduction peak is explained by the amount of chemisorbed oxygen on the cathode electrode surface. It is already discussed that a diffusion layer is established as the oxygen molecules transfer from the bulk to the electrode surface. The diffusion layer size depends on the voltage scan rate. At a slow scan rate, the diffusion layer will be given ample time to create a thicker layer than the quick scanning rate. The diffusion of oxygen at the electrode surface is thereby significantly decreased at a low scan rate (Pramanik and Basu 2011). It was evident in Figure 5.18, that CVs with a scanning rate of 100 mV/s generate prominent peaks of oxygen reduction for Pt-Ni/C_{AB}-DMSO, Pt-Ni/C_{AB}-DMF and Pt-Ni/C_{AB}-EG at peak position − 0.13 V, + 0.33 V and + 0.43 V with corresponding current density 8.28 mA/cm^2, 0.78 mA/cm^2 and 1.80 mA/cm^2, respectively. The ORR peak for electrocatalyst Pt-Ni/C_{AB}-EG was observed in a more positive direction as compared to other two Pt-Ni/C_{AB}-DMSO and Pt-Ni/C_{AB}-DMF

electrocatalyst, which indicates electrocatalyst Pt-Ni/C_{AB}-EG has comparatively lower activation losses for ORR.

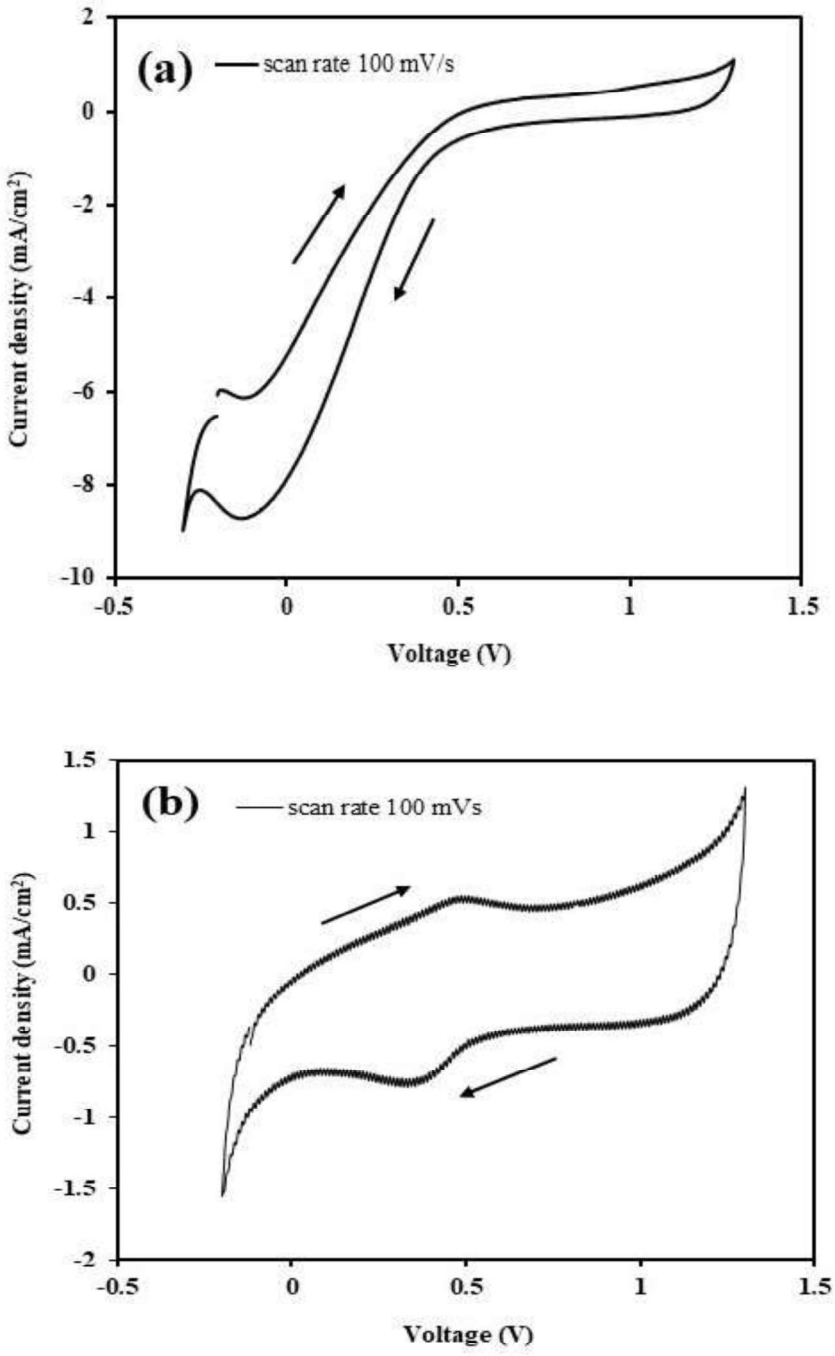

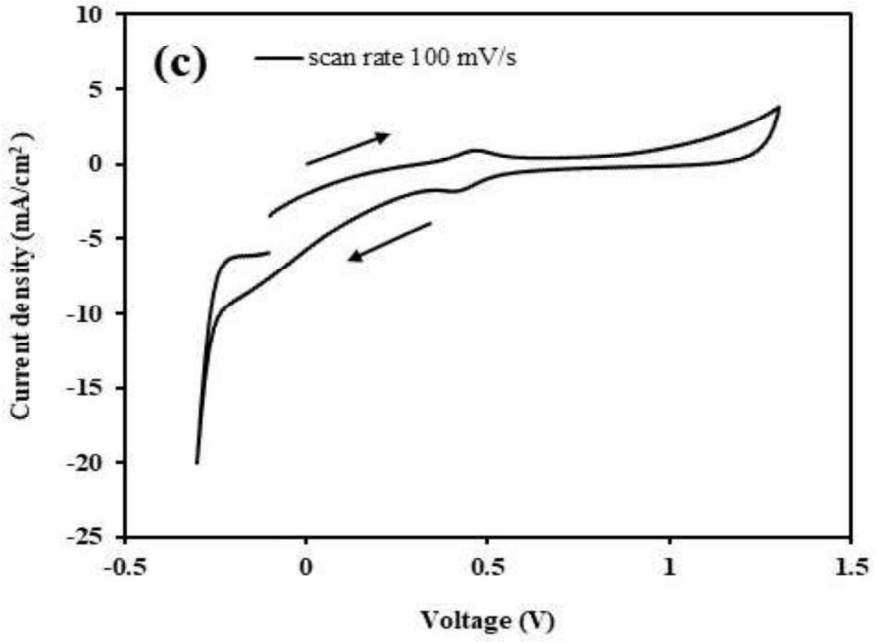

Figure 5.18 Cyclic voltammetry for synthesized electrocatalysts (a) Pt-Ni/C_{AB}-DMSO, (b) Pt-Ni/C_{AB}-DMF and (c) Pt-Ni/C_{AB}-EG of fixed loading 1 mg/cm^2 with 100 mV/s scan rate using oxygen saturated 0.5 M $HClO_4$ electrolyte; temperature 30 ^oC.

5.2.3 Performance study of synthesized Pt-Ni(3:1)/CAB electrocatalyst in single cell PEMFC

5.2.3.1 Effect of cathode electrocatalyst type

Figure 5.19 shows the polarization and power density characteristics curves for cathode electrocatalyst Pt-Ni/C_{AB}-DMSO, Pt-Ni/CAB-DMF and Pt-Ni/C_{AB}-EG. The electrocatalytic activity of the synthesized cathode electrocatalyst was investigated in the PEMFC single cell setup. The anode electrocatalyst loading was kept fixed at 1 mg/cm^2 of commercial electrocatalyst Pt/C_{HSA}. For each set of experiments, the cathode was fabricated of synthesized electrocatalyst Pt-Ni/C_{AB}-DMSO or Pt-Ni/C_{AB}-DMF or Pt-Ni/C_{AB}-EG of 1 mg/cm^2 of each electrocatalyst. To determine the best cathode electrocatalyst in terms of cell performance, the PEMFC was operated at a room temperature of 33 ^oC. The synthesized cathode Pt-Ni(1:3)/C_{AB}-EG produced the maximum open circuit voltage (OCV) of 0.909 V and the maximum power density of 25.60

mW/cm^2 at a current density of 64 mA/cm^2, whereas Pt-Ni/C_{AB}-DMSO and Pt-Ni/C_{AB}-DMF produced OCVs of 0.910 V and 0.911 V, respectively. The PEMFC setup produced maximum power density of 25.60 mW/cm^2, 11.33 mW/cm^2, and 6.70 mW/cm^2 for the cathode electrocatalyst Pt-Ni/C_{AB}-EG, Pt-Ni/C_{AB}-DMF, and Pt-Ni/C_{AB}-DMSO, respectively. The electrocatalyst (Pt-Ni/C_{AB}) synthesized in atomic ratio of 1:1 and 1:3 using different solvent (DMSO or DMF or EG) also come up with poor performance as compared to Pt-Ni(3:1)/C_{AB}-EG. The polarization and power density cures for the other atomic ratios of Pt to Ni are presented in Appendix D (Figure D3 to Figure D4). The PEMFC performance in term of power density clearly indicates that the Pt-Ni/C_{AB}-EG cathode electrocatalyst exhibits higher activity for ORR as compare to Pt-Ni/C_{AB}-DMSO and Pt-Ni/C_{AB}-DMF electrocatalyst. It is possible due to the fact that Pt-Ni/C_{AB}-EG electrocatalyst has the smallest particle size, resulting in a very large active surface area for ORR. In addition as discussed in section 5.2.2.1, lower activation loss of Pt-Ni/C_{AB}-EG confirms the reason of higher activity (Singh and Pramanik 2022). Another factor for the superior performance of Pt-Ni/C_{AB}-EG electrocatalyst is the highest degree of Pt alloying (7.47 %) in the Pt-Ni alloy compared to Pt-Ni/C_{AB}-DMSO (6.22 wt. %) and Pt-Ni/C_{AB}-DMF (6.22 wt. %) (Hyun et al., 2013).

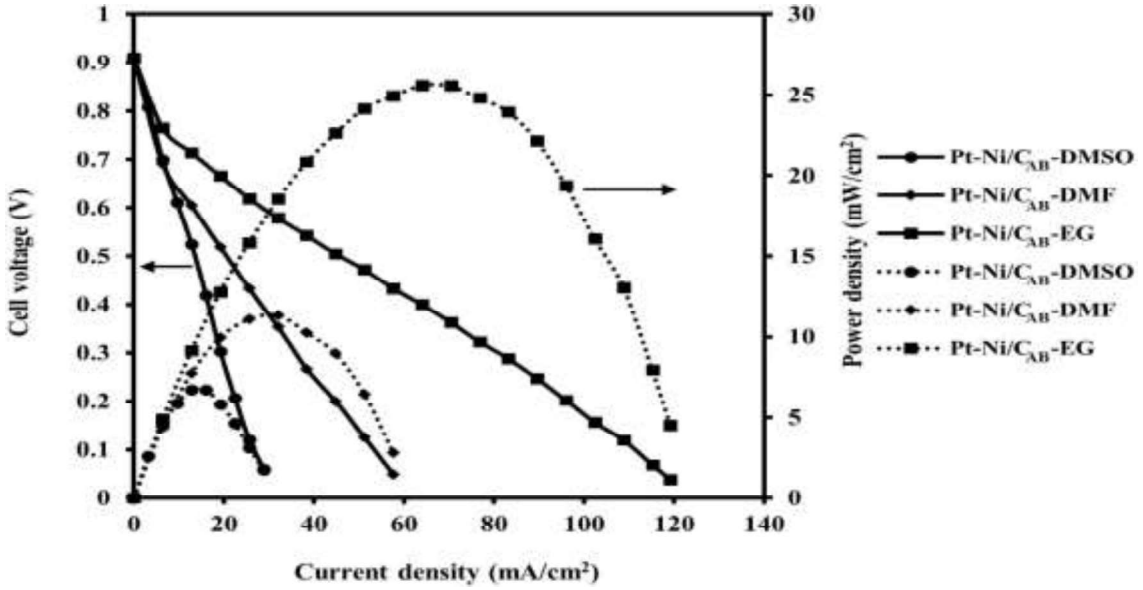

Figure 5.19 Polarization and power density curves for commercial anode Pt/C_{HSA} electrocatalyst of loading 1 mg/cm^2 and synthesized cathode Pt-Ni/C_{AB}-DMSO, Pt-Ni/C_{AB}-DMF and Pt-Ni/C_{AB}-EG electrocatalysts of loading 1 mg/cm^2 respectively, in proton exchange membrane fuel cell at operating temperature of 33 ºC; Dotted line – power density curves; Solid lines – polarization curves.

5.2.3.2 Effect of anode loading

The effect of anode loading was investigated taking commercial Pt/C_{HSA} anode and synthesized Pt-Ni(3:1)/C_{AB}-EG best electrocatalyst as cathode electrocatalyst. The commercial electrocatalyst Pt/C_{HSA} (40 wt. %) loading at anode was varied from 0.75 mg/cm^2 to 1.25 mg/cm^2. The synthesized Pt-Ni/C_{AB}-EG demonstrated the best cell performance in terms of power density as it is shown in the previous section, thus it was chosen as the cathode electrocatalyst for anode loading optimization (Figure 5.20). The cathode loading of synthesized Pt-Ni/C_{AB}-EG electrocatalyst was kept fixed at 1 mg/cm^2. The single cell PEMFC study confirms that the 1 mg/cm^2 loading produced highest enhanced the output in terms of current density and power density in comparison to other electrocatalyst loading i.e., 0.75 mg/cm^2 and 1.25 mg/cm^2. The maximum OCV of 0.909 V was observed for anode loading of 1mg/cm^2, which was slightly higher than OCVs observed for other

anode loading i.e., 0.905 V and 0.903 V for loading of 0.75 mg/cm^2 and 1.25 mg/cm^2, respectively. The highest power density of 25.60 mW/cm^2 at a current density of 64 mA/cm^2 was obtained at anode loading of 1 mg/cm^2, which is highest of all anode loading. The anode loading of 0.75 mg/cm^2 and 1.25 mg/cm^2 produced maximum power density of 19.58 mW/cm^2 and 20.28 mW/cm^2, respectively. The reason for higher performance with the increase in the electrocatalyst loading upto 1 mg/cm^2, may be due to the increase in the active surface area and suitable porosity available for the mass transfer of reactants from bulk to the electrocatalyst surface. However, beyond the loading 1 mg/cm^2, the cell performance got decrease and it may be due to the increased diffusion mass transfer resistance due to agglomeration of anode electrocatalyst, which decreases the active sites for anode electrode as well as impedes the flow of hydrogen fuel from anode side electrode surface to cathode side electrode at very high loading (1.25 mg/cm^2) (Pramanik and Rathoure 2017).

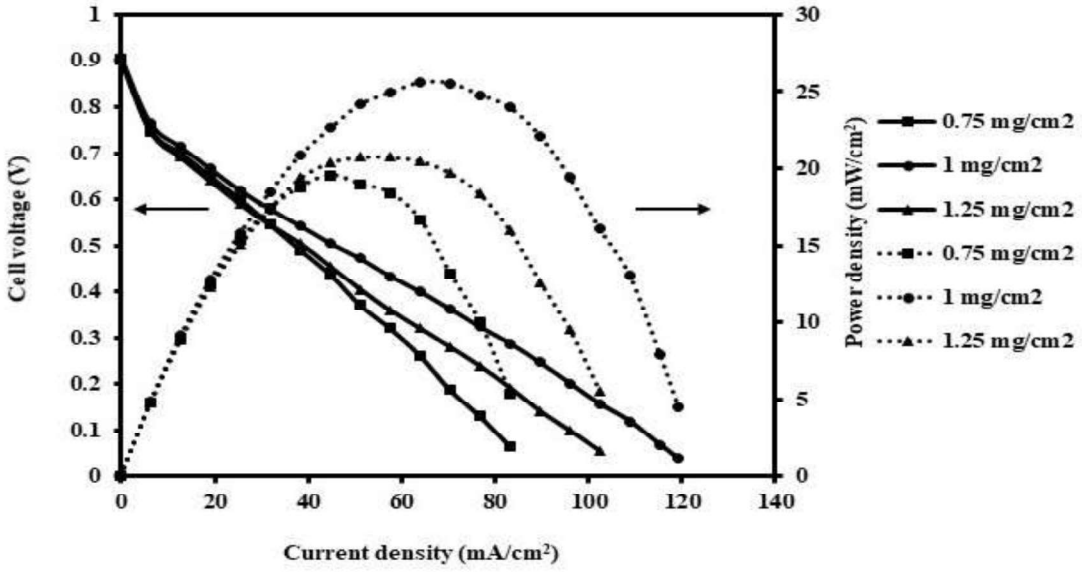

Figure 5.20 Polarization and power density curves for varying loading of commercial anode Pt/C_{HSA} electrocatalyst and fixed loading of 1 mg/cm^2 synthesized Pt-Ni/C_{AB}-EG cathode electrocatalyst in proton exchange membrane fuel cell at operating temperature of 33 ^oC; Dotted line – power density curves; Solid lines – polarization curves.

5.2.3.3 Effect of cathode loading

5.2.3.3.1 Pt-Ni(3:1)/C_{AB}-EG as cathode electrocatalyst

The cathode loading Pt-Ni/C_{AB}-EG was varied from 0.75 mg/cm^2 to 1.25 mg/cm^2 to find out the optimum loading of cathode. The anode electrocatalyst loading of 1 mg/cm^2 was kept fixed at anode side. The polarization and power density curves for varying cathode loadings is shown in Figure 5.21. The polarization and power density curves shifted upward when cathode loading was increased from 0.75 mg/cm^2 to 1 mg/cm^2. However, the curves shifted downward when the cathode loading was increased further to 1.25 mg/cm^2. The reason for such trend with the increase in electrocatalyst loading is already discussed in the section 5.2.3.2. Figure 5.21 shows that the optimum cathode loading of 1 mg/cm^2 resulted in the highest cell performance in terms of power density i.e., 25.60 mW/cm^2 at a current density of 64 mA/cm^2. However, the maximum power densities of 14.52 and 17.02 mW/cm^2 were obtained for cathode loadings of 0.75 mg/cm^2 and 1.25 mg/cm^2 at current densities of 38.4 mA/cm^2 and 44.8 mA/cm^2, respectively. In terms of OCV and power density, Pt-Ni/C_{AB}-EG showed significance performance as compare to other synthesized cathode electrocatalysts i.e., Pt-Ni/C_{AB}-DMSO and Pt-Ni/C_{AB}-DMF.

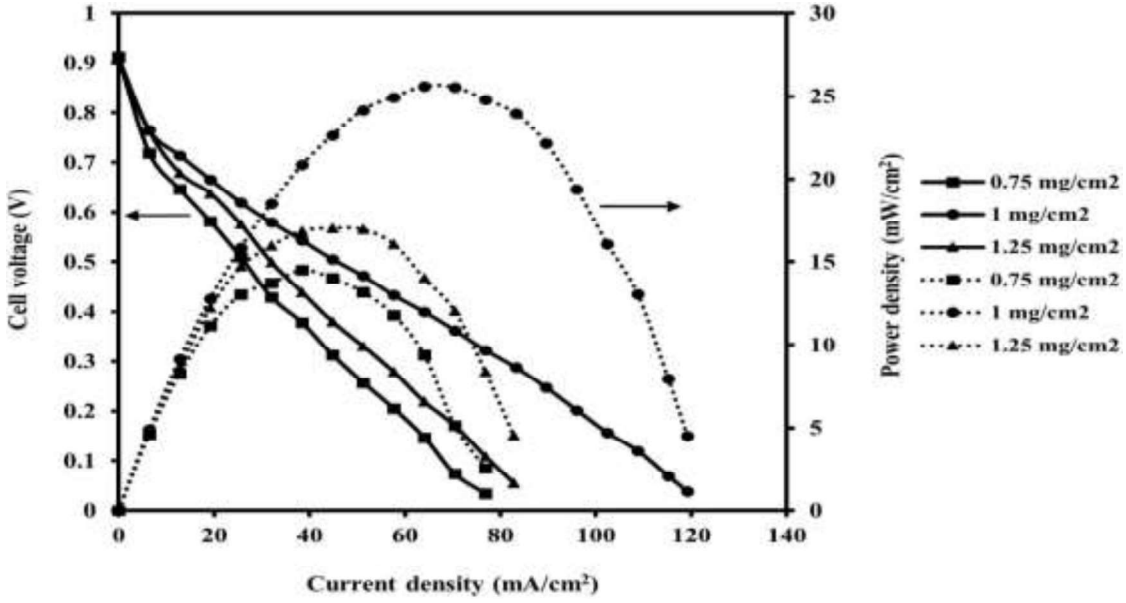

Figure 5.21 Polarization and power density curves for commercial anode Pt/C_{HSA} electrocatalyst of loading 1 mg/cm^2 and synthesized cathode Pt-Ni/C_{AB}-EG electrocatalysts of loading 1 mg/cm^2 respectively, in proton exchange membrane fuel cell at operating temperature of 33 ^oC; Dotted line – power density curves; Solid lines – polarization curves.

5.2.3.3.2 Pt-Ni(3:1)/C_{AB}-DMF as cathode electrocatalyst

Figure 5.22 shows the performance of PEMFC using Pt-Ni/C_{AB}-DMF as cathode electrocatalyst of varying loading in the range of 0.75 mg/cm^2 to 1.25 mg/cm^2. Figure 5.22 indicates that the cell performance increases with the increase in cathode loading from 0.75 mg/cm^2 to 1 75 mg/cm^2. Further increase in cathode loading beyond 1 mg/cm^2, the cell performance declined. The maximum power density of 11.33 mW/cm^2 at a current density of 32 mA/cm^2 was obtained at the cathode electrocatalyst loading of 1 mg/cm^2. Lowest power density of 8.03 mW/cm^2 at a current density of 19.2 mA/cm^2 was produced at the lowest electrocatalyst loading of 0.75 mg/cm^2. While the maximum power density of 9.37 mW/cm^2 was obtained at current density of 19.2 mA/cm^2. It should be noted that the highest power density (11.33 mW/cm^2) produced by the Pt-Ni/C_{AB}-DMF at the optimum loading was lower than the maximum power density (25.60 mW/cm^2) produced by the Pt-Ni/C_{AB}-EG at the optimum loading of 1 mg/cm^2. The reason for highest performance at

the optimum loading of 1 mg/cm^2 is already discussed in section 5.2.3.3.2 (Page no. 108). Beyond the optimum loading, the electrocatalyst layer become very compact and thus, it prevents oxygen molecules from diffusing freely at the cathode electrode surface, which significantly affect the PEMFC performance in term of power density.

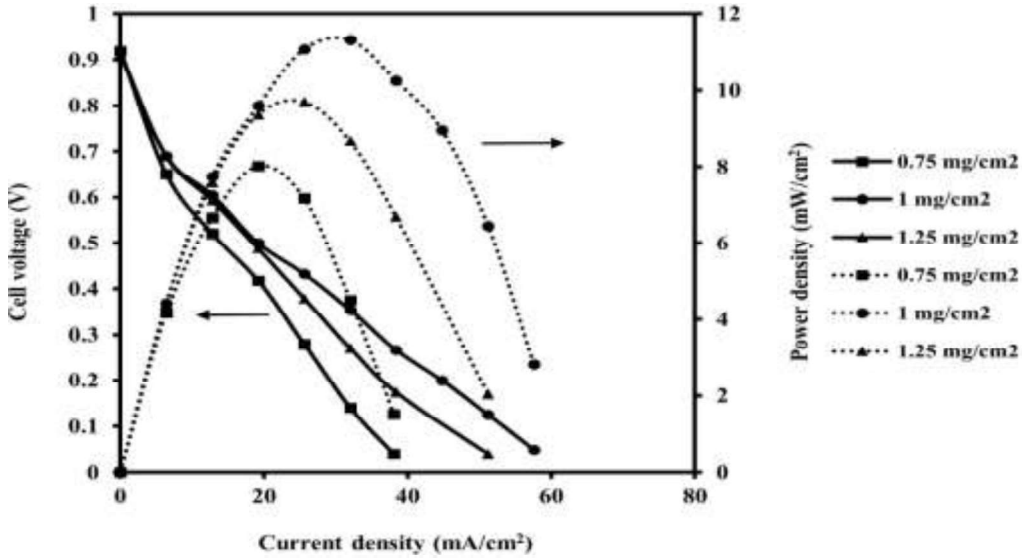

Figure 5.22 Polarization and power density curves for commercial anode Pt/C_{HSA} electrocatalyst of loading 1 mg/cm^2 and synthesized cathode Pt-Ni/C_{AB}-DMF electrocatalysts of loading 1 mg/cm^2 respectively, in proton exchange membrane fuel cell at operating temperature of 33 ºC; Dotted line – power density curves; Solid lines – polarization curves.

5.2.3.3.3 Pt-Ni(3:1)/C_{AB}-DMSO as cathode electrocatalyst

Figure 5.23 shows performance of the Pt-Ni/C_{AB}-DMSO cathode electrocatalyst with varying cathode loading ranging from 0.75 mg/cm^2 to 1.25 mg/cm^2. It is seen from Figure 5.23 that the PEMFC performance increases with increase in the cathode loading upto 1 mg/cm^2. However, with the increase in loading beyond 1 mg/cm^2, the performance of the cell decreases. The cathode loading at 1 mg/cm^2 produced the highest power density of 6.07 mW/cm^2, which is lower than the Pt-Ni/C_{AB}-EG (25.60 mW/cm^2) and Pt-Ni/C_{AB}-DMF (11.33 mW/cm^2) cathode produced at their optimum loading. The cathode electrocatalyst Pt-Ni/C_{AB}-DMSO with very low loading of 0.75

mg/cm^2 and very high loading of 1.25 mg/cm^2 produced maximum power density of 5.34 mW/cm^2 and 5.61 mW/cm^2, respectively. The highest power density obtained at the loading of 1 mg/cm^2, may be due to an excellent compromise between the accessible cathode surface and electrocatalyst metal particle availability without any agglomeration.

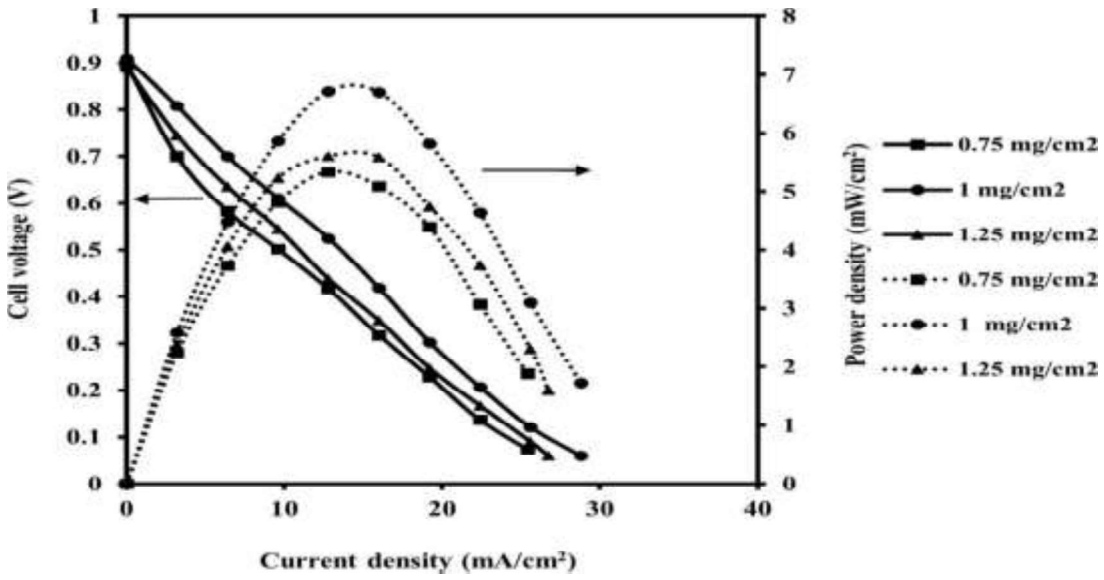

Figure 5.23 Polarization and power density curves for commercial anode Pt/C_{HSA} electrocatalyst of loading 1 mg/cm^2 and synthesized cathode Pt-Ni/C_{AB}-DMSO electrocatalysts of loading 1 mg/cm^2 respectively, in proton exchange membrane fuel cell at operating temperature of 33 ºC; Dotted line – power density curves; Solid lines – polarization curves.

5.2.3.4 Effect of temperature in PEMFC

Figure 5.24 shows the effect of cell temperature on the polarization and power density characteristics for commercial anode (Pt/C_{HSA}) electrocatalyst loading of 1 mg/cm^2 (optimum) and synthesized cathode Pt-Ni/C_{AB}-EG loading of 1 (optimum) using varying temperature ranging from 33 ºC to 70 ºC. It is seen from the Figure 5.24 that polarization and maximum power density curves shifted up with the increases in temperature from 33 ºC to 60 ºC. However, both the curves shifted downward beyond the temperature 60 ºC. In order to avoid dehydration of the PEM electrolyte and electrode catalyst layer, the temperature of the PEMFC was not raised above 70

ºC. The increase in cell performance with the increase in temperature may be due to the reduction in activation losses and faster reaction kinetics at both the electrodes (Singh and Pramanik 2024). As per literature, high temperatures (T <80 ºC), the proton conductivity of the Nafion® membrane was substantially improved and lowered ohmic loss (Alzate et al., 2011). Furthermore, little high cell operating temperature also increase the mass transmission rate of reactants and thus, decrease concentration loss (Goel and Basu 2012). The PEMFC working at a room temperature of 33 °C, the maximum power density of 25.60 mW/cm^2 was obtained. However, the maximal power density of 42.29 mW/cm^2 was obtained when the cell performance was increased to 60 ºC. As the cell operating temperature is raised from 33 °C to 60 °C, the maximum power density improved dramatically, i.e., about 65.19 %. It should be noted that at very high temperature at about 70 ºC, the PEMFC performance in term of power density got decreased (83.2 mW/cm^2) (Table 5.12). It may be due to the dying effect of the electrodes (Yadav and Pramanik 2024).

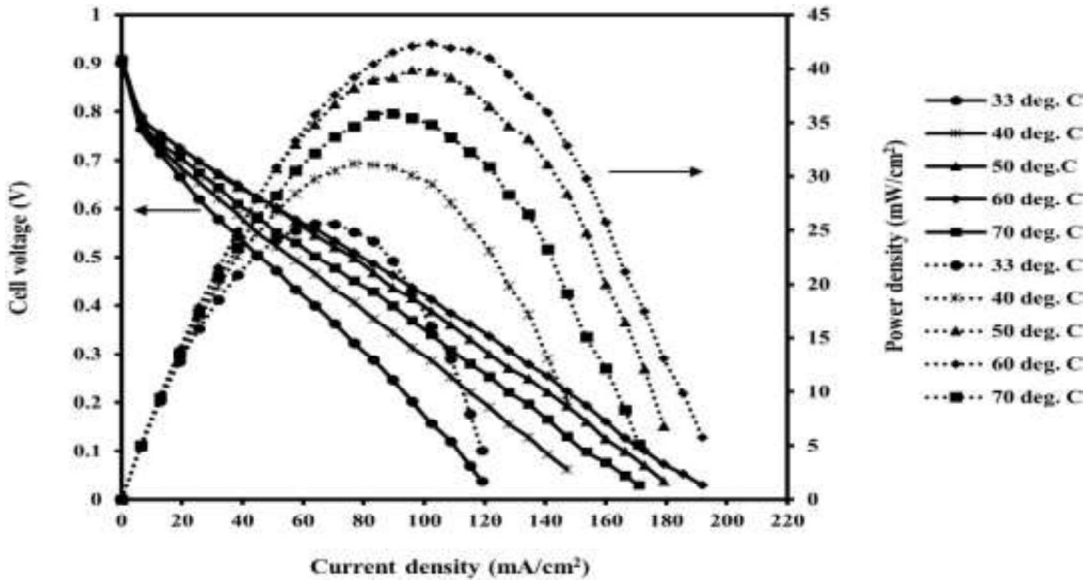

Figure 5.24 Polarization and power density curves for commercial anode Pt/C_{HSA} electrocatalyst and synthesized Pt-Ni/C_{AB}-EG cathode electrocatalyst keeping fixed both loading at 1 mg/cm^2; Dotted line – power density curves; Solid lines – polarization curves.

Table 5.12 Summary of performance of the synthesized best cathode Pt-Ni/C_{AB}-EG electrocatalyst using optimum loading of 1 mg/cm^2 in a proton exchange membrane fuel cell (PEMFC) at various operating temperatures.

Temperature (ºC)	OCV (V)	Maximum power density (mW/cm^2)	Current density at maximum power density (mA/cm^2)
33	0.909	25.60	64
40	0.909	31.18	76.8
50	0.907	39.84	96
60	0.904	42.29	102.4
70	0.901	35.69	83.2

As discussed in the sections titled "5.1 Pt-Co(3:1)/C_{AB} cathode electrocatalyst performance evaluation: Part I" and "5.2 Pt-Ni(3:1)/C_{AB} cathode electrocatalyst performance evaluation: Part II, " the Pt-Ni/C-EG electrocatalyst showed the best performance among all synthesized bimetallic cathode electrocatalyst i.e., Pt-Co/C_{AB} and Pt-Ni/C_{AB}. Thus, synthesized cathode Pt-Ni/C-EG electrocatalyst was chosen to develop a mathematical model for optimization of the effective process parameters of the single PEMFC using a very popular statistical method response surface methodology (RSM) in the proceeding section. The develop method was also validated using experimental data.

5.2.4 Process parameter optimization using RSM

5.2.4.1 ANOVA and model development

Table 5.13 shows the power density (Y) as a result of synthesized Pt-Ni(3:1)/C_{AB}-EG electrocatalyst in single PEMFC. Table 5.13 also shows the predicted values of power densities from the model and the actual values of power densities from experiments.

Table 5.13 The BBD arrangement for PEMFC and the corresponding experimental and predicted power density.

Run	A- Cathode electrocatalyst loading (mg/cm^2)	B- Cell temperature (^{o}C)	C- H_2 flow rate (ml/min)	Actual predicted power density (mW/cm^2)	Experimental power density (mW/cm^2)
1	1	50	40	20.89	21.30
2	1	60	50	42.29	42.29
3	0.75	70	50	23.73	23.74
4	0.75	50	50	21.33	20.83
5	1	60	50	42.29	42.29
6	0.75	60	40	18.33	18.42
7	1	50	60	22.23	22.33
8	0.75	60	60	21.76	22.16
9	1.25	60	60	22.12	22.03
10	1	60	50	42.29	42.29
11	1.25	60	40	20.43	20.03
12	1	60	50	42.29	42.29
13	1.25	70	50	23.70	24.20
14	1	70	60	27.19	26.78
15	1	60	50	42.29	42.29
16	1	70	40	22.18	22.08
17	1.25	50	50	21.89	21.88

The operating cell voltage and corresponding maximum power density for all 17 experiments obtained from BBD arrangements is presented in Appendix F. To calculate the power density (Y) in the PEMFC, a second order polynomial regression given by Equation (5.6) was obtained from RSM:

$$\text{Power density (Y)} = -709.24875 + 367.17500\,A + 10.03000\,B + 10.35188\,C - 0.059000\,A\times B - 0.174000\,A\times C + 0.009175\,B\times C - 176.72000\,A^2 - 0.085825\,B^2 - 0.105850\,C^2 \quad (5.6)$$

Where A represents the cathode electrocatalyst loading (mg/cm^2), B cell temperature (^{o}C), and C hydrogen flow rate (ml/min). The predicted values of power density (Y) are determined using the actual data of the input parameters. The coefficient with positive values in Equation (5.6) implies that these components influence the response positively. The terms with negative coefficients, on the other hand, are incompatible with the response. The positive coefficient terms in the model equation associated with A, B, C and BC have a positive effect on response. Whereas, negative coefficient terms associated with, such as AB, AC, A^2, B^2 and C^2 have a negative effect on the response.

When the PEMFC was operating with cathode electrocatalyst loading of 1 mg/cm^2, cell temperature of 60 ^{o}C and hydrogen flow rate of 50 ml/min, the highest maximum power density of 42.29 mW/cm^2 was obtained. The lowest power density of 18.42 mW/cm^2 was observed at 0.75 mg/cm^2 cathode electrocatalyst loading, cell temperature of 60 ^{o}C and hydrogen flow rate of 40 ml/min. Table 5.13 shows the predicted power maximum density and experimental maximum power density of all 17 experiments under various cell conditions. The statistical analysis for the power density of the hydrogen based PEMFC from the analysis of variance (ANOVA) using the

quadratic model is shown in Table 5.14. The source is the name of column, the sum of squared is the deviation from the mean, and Df is the degree of freedom for the model, which signifies the model terms plus the intercepts minus one. The mean square (MS) is the sum of squares to the Df ratio that estimates the model variance. The F-value for each term is the test for determining the relationship between the variance associated with that term and the residual variance.

Table 5.14 ANOVA of the fitted quadratic model for the response.

Source	Sum of squares (SS)	Df	Mean square (MS)	F value	p-value; prof>F	Remarks
Model	1204.37	9	133.82	797.27	< 0.0001	significant
A- Cathode loading	1.12	1	1.12	6.66	0.0365	……..
B- Cell temperature	13.68	1	13.68	81.48	< 0.0001	……..
C- H_2 flow rate	16.45	1	16.45	97.98	< 0.0001	……..
AB	0.0870	1	0.0870	0.5185	0.4948	……..
BC	0.7569	1	0.7569	4.51	0.0713	……..
AC	3.37	1	3.37	20.06	0.0029	……..
A^2	422.74	1	422.74	2518.60	< 0.0001	……..
B^2	240.49	1	240.49	1432.78	< 0.0001	……..
C^2	384.82	1	384.82	2292.66	< 0.0001	…….
Residual	1.17	7	0.1678	……..	……..	……..
Lack of fit	1.17	3	0.3916	……..	……..	Not significant
Pure error	0.0000	4	0.0000	……..	…….	…….
Cor total	1205.55	16	…….	……..	……..	…….
R^2	0.9992	..……	……	...…..	..……..	……..
Adjusted R^2	0.9982	……	……..	…..…	..……..	……..
Predicted R^2	0.9873	……	……..	……..	..……	……

F-value is the ratio of the mean square of the term to the mean square for the residual. The p-value for this model is 0.0001 and the F-value is 797.27 which is greater than 1. Thus, the ANOVA fitted Quadratic Model is significant. The significant process parameters, namely cell temperature (B) and hydrogen flow rate (C) had p-values of 0.0001, and 0.0001while the p-value of 0.0365 for cathode loading (A) is slightly significant according to the model. The second-order model equation, which relates dependent and independent parameters, was produced in terms of actual elements were shown in Equation 5.6. The Predicted R-Squared value is 0.9873, which is in good agreement with the Adjusted R-Squared value of 0.9982 (Choudhary and Pramanik 2021).

The relationship between the actual data of power density received from the experiments graph and the predicted data from the model is shown in Figure 5.25, where the point of the actual power density of the experiment is near to the predicted values of power density. The power density produced from the experiments had an orderly distribution, as it is shown by this graph Figure 5.25, with a linear direction, indicating that this model can accurately predict the response in term of power density which, may satisfied the model. According to Table 5.14, there is a difference of less than 0.02 between the predicted and adjusted R^2 values for this model, which implies that the non-significant terms have no impact on the quadratic model. The R^2 coefficient value for this model is 0.9992, which shows that model well fitted the experimental data.

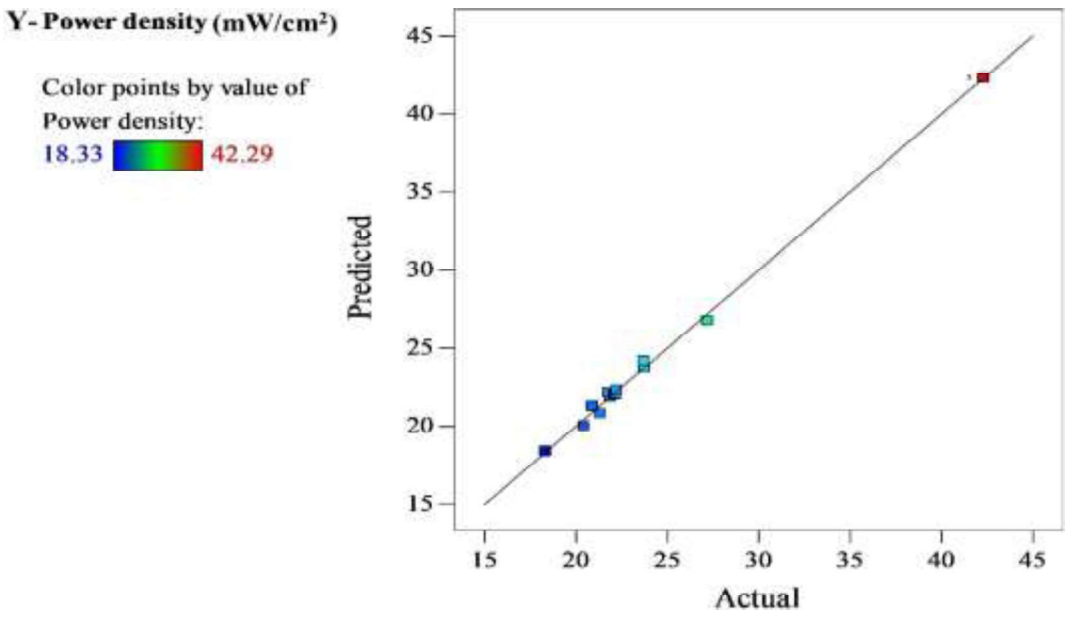

Figure 5.25 Actual versus model predicted power density comparison.

Figure 5.26 displays the expected vs. residual graph. The residual values are the outcomes of the difference between experimental and predicted values. It shows the predictability. Figure 5.26 shows that the values on the Y-axis from the positive side indicate that the expected value was too low. While the higher expected values are presented on the negative side of the Y-axis. The values near the X-axis indicate that the experiment values are close to the predicted values.

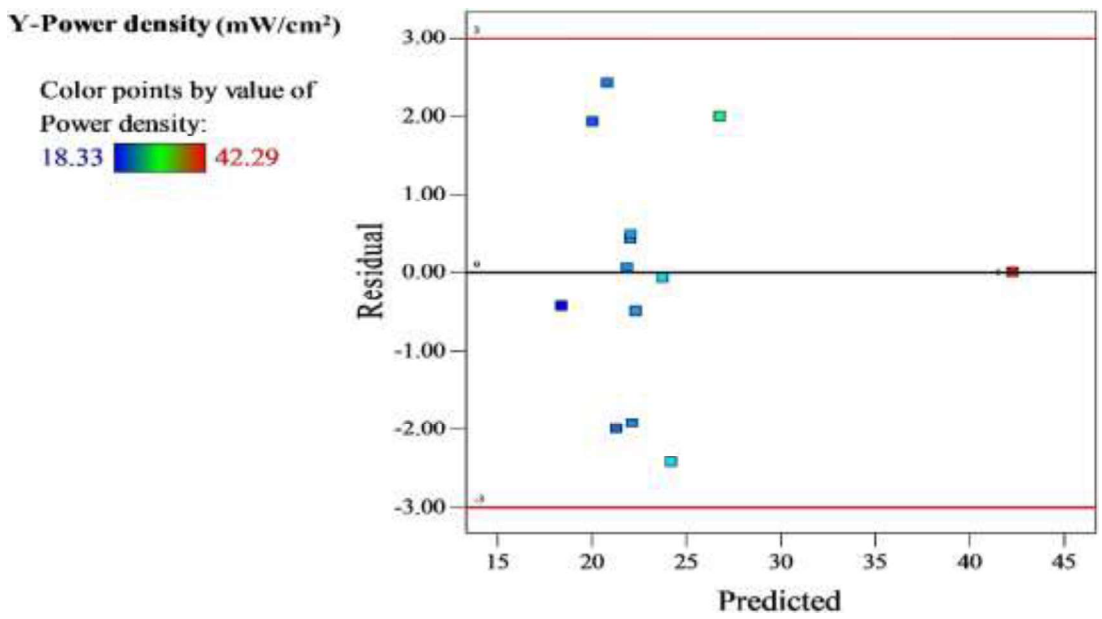

Figure 5.26 Predicted vs. Residual value of power density obtained from PEMFC.

5.2.4.2 Process parameter optimization and its effect on response

The 3D surface plot of the response in term of power density as a function of two independent variables (A) and (C), while holding the third variable (B) constant, is shown in Figures 5.27(a-c). The two test variables are divided into an infinite number of groups while the other one is maintained in all 3D plots fixed. To create 3D graphs between the process parameters, and the response the polynomial regression Equation (4.2) was employed. Oxygen was used as oxidant at cathode side and hydrogen was used as fuel at anode side for all experiments. All experiments are performed at Pt/C_{HSA} anode electrocatalyst with a fixed loading of 1 mg/cm^2. The values of the power density (Y), as indicated by the surface, are represented by the various color codes of the 3D plot. The effect of the cathode electrocatalyst loading (A) and cell temperature (B) on the power density (Y) at fixed hydrogen flow rate (C) of 49.96 ml/min is shown in Figure 5.27a. The peak power density rises with the increase in cell temperature (B) upto 60.84 ^oC and cathode electrocatalyst loading (A) from 0.75 to 0.99 mg/cm^2. However, a further increase in the cathode

electrocatalyst loading (A) beyond 0.99 mg/cm^2 and cell temperature (B) beyond 60.84 ºC power density begins to decrease. The decrease in power density of PEMFC at higher anode loading of 1.5 mg/cm^2 can be due to electrocatalyst particle agglomeration/compaction in a limited region and a rise in electrode thickness. This reduces the number of active electrocatalyst sites per unit area and the porosity of the electrode electrocatalyst layer (Panjiara and Pramanik 2022; Singh et al., 2022).

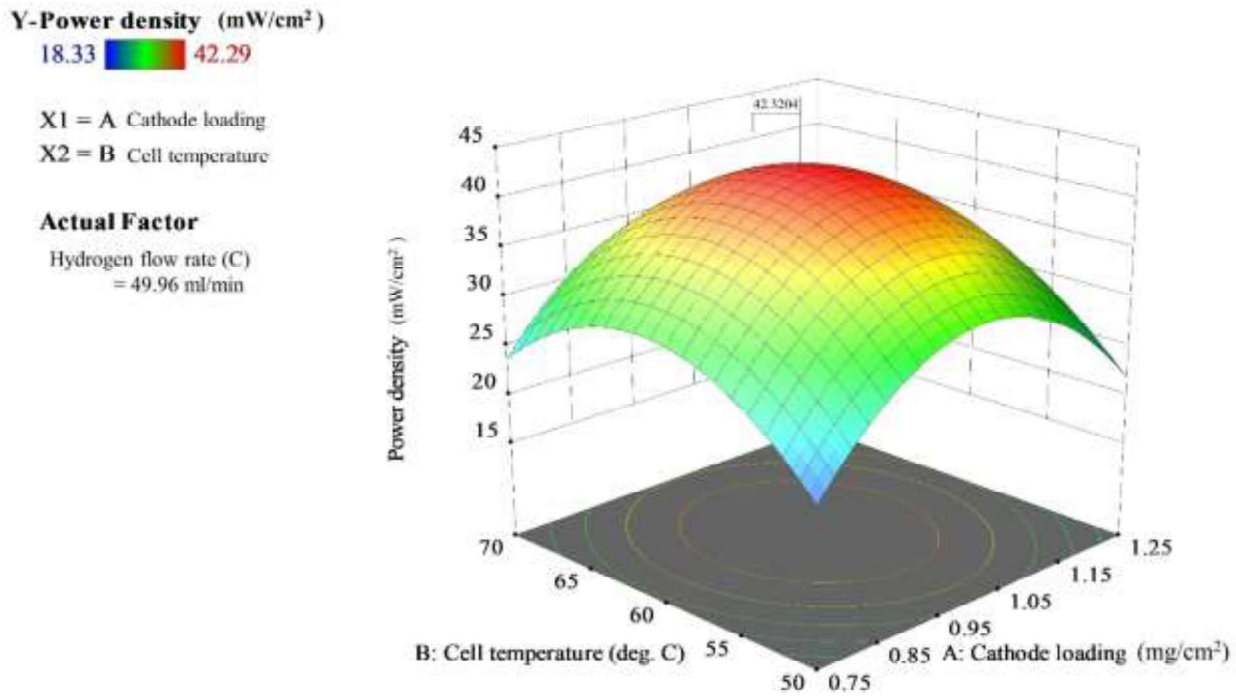

Figure 5.27a Three-dimensional (3D) response plots showing the effect of cathode loading (A), cell temperature (B) and their mutual interaction on power density.

Figure 5.27b represents 3D surface interaction response plot in term of power density (Y) as a function of two independent variables cathode electrocatalyst loading (A) and hydrogen flow rate (C) at fixed cell temperature (B) of 60.84 ºC. The power density increases with the increase in cathode loading (A) up to 0.99 mg/cm^2 and hydrogen flow rate (C) 49.96 ml/min and achieved the peak power density of 42.32 mW/cm^2. However, a further increase in cathode electrocatalyst

loading beyond 0.99 mg/cm^2 and hydrogen flow rate beyond 49.96 ml/min leads to decreasing trend in power density generation, this characteristic nature of power density (Y) at high hydrogen flow rate (C) beyond 49.96 ml/min is due to hydrogen gas crossover across the cathode side of PEMFC. This causes a fall in cell voltage and a considerable loss in power density (Yun et al., 2018). It was found that not only the hydrogen flow rate but also the cathode electrocatalyst loading has a significant influence in the power density where excess loading leads to agglomeration of active sites and increase in ohmic impedance.

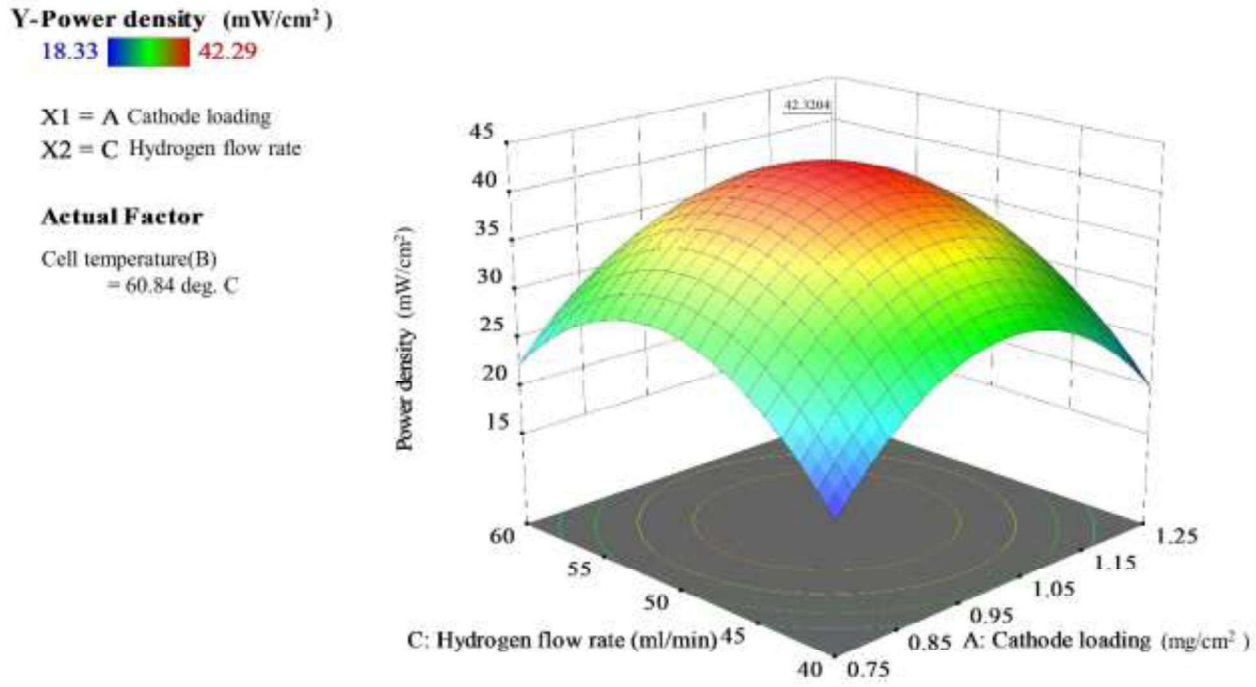

Figure 5.27b Three-dimensional (3D) response plots showing the effect of cathode loading (A), hydrogen flow rate (C) and their mutual interaction on power density.

Figure 5.27c represents the 3D response surface plot which shows the effect of cell temperature (B) and hydrogen flow rate (C) on the power density (Y) at fixed cathode electrocatalyst loading (A) of 0.99 mg/cm^2. As the cell temperature (B) rises up to 60.84 ^{o}C along with hydrogen flow

rate increasing upto 49.97 ml/min, the power density (Y) rises to 42.32 mW/cm^2. However, a further increase in cell temperature (B) and hydrogen flow rate (C) beyond 0.99 mg/cm^2 and 49.97 m/min the power density (Y) deceases rapidly. Due to increasing the cell temperature the Arrhenius equation leads to enhanced electrocatalytic reaction kinetics for better performance of PEMFC in terms of power density (Singh et al., 2023), as well as raising the operating temperature of PEMFC enhances conductivity of nafion membrane (Yadav and Pramanik 2023; Goel and Basu 2012). However, at higher operating cell temperatures beyond 60.84 ºC, the nafion membrane dehydrates rapidly, which reduces PEMFC performance because hydronium ions are limited (Okonkwo et al., 2021). Figure 5.27c also shows that the power density (Y) is strongly impacted by operating cell temperature (B) hydrogen flow rate (C).

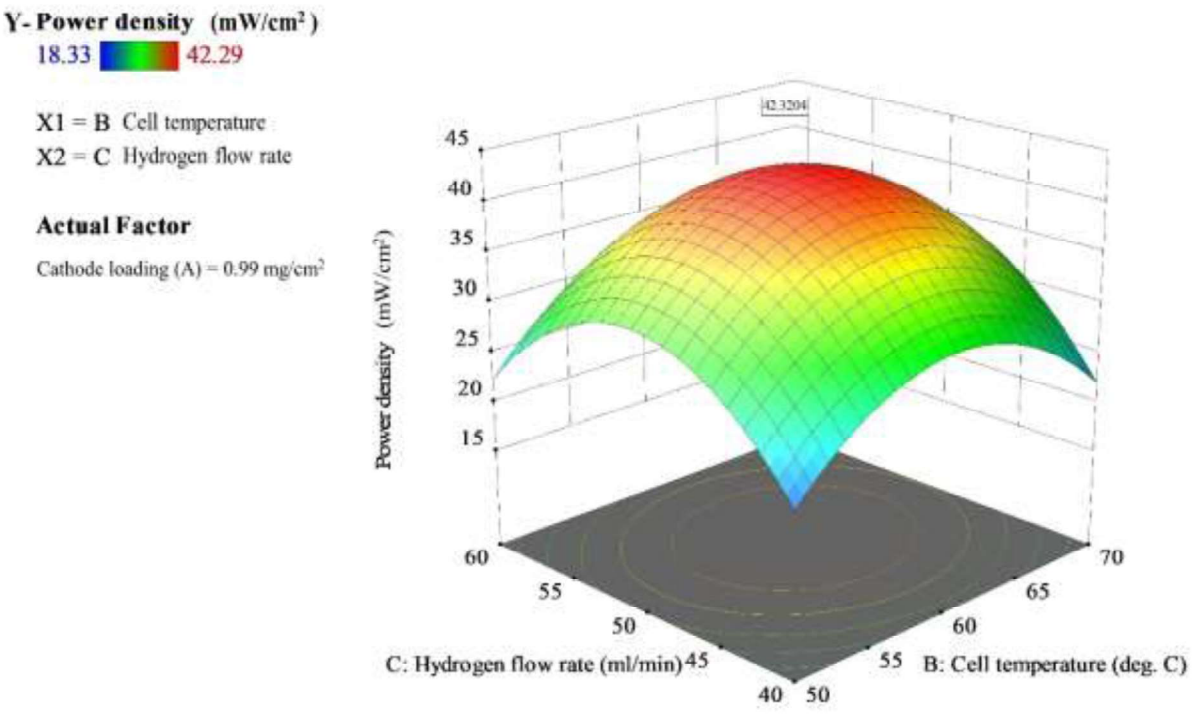

Figure 5.27c Three-dimensional (3D) response plots showing the effect of cell temperature (B), hydrogen flow rate (C) and their mutual interaction on power density.

5.2.4.3 Polarization and power density curves

To obtain the maximum power density at the predicted operating conditions, experiments was performed which gives cell voltage and current density data followed by polarization and power density curves as it is shown in the Figure 5.28a. To compare the actual and predicted values of power density, the polarization curve on the optimum condition of parameters obtained from RSM analysis is shown in Figure 5.28a. The polarization and power density curves for hydrogen-based PEMFC using cathode electrocatalyst Pt-Ni/C_{AB}-EG was tested at its optimum operating conditions. The cathode electrocatalyst loading (A) of 0.99 mg/cm^2, cell temperature (B) of 60.84 ^oC, and hydrogen flow rate of 49.96 ml/min are the optimum conditions as determined by RSM studies. To establish the PEMFC consistent polarization behavior, all experiments were conducted three times. The polarization curves of three tests that were carried out repeatedly at optimum conditions. Table 5.15 shows the actual/experimental value of power density obtained at the optimum condition and comparison of the same with the predicted value.

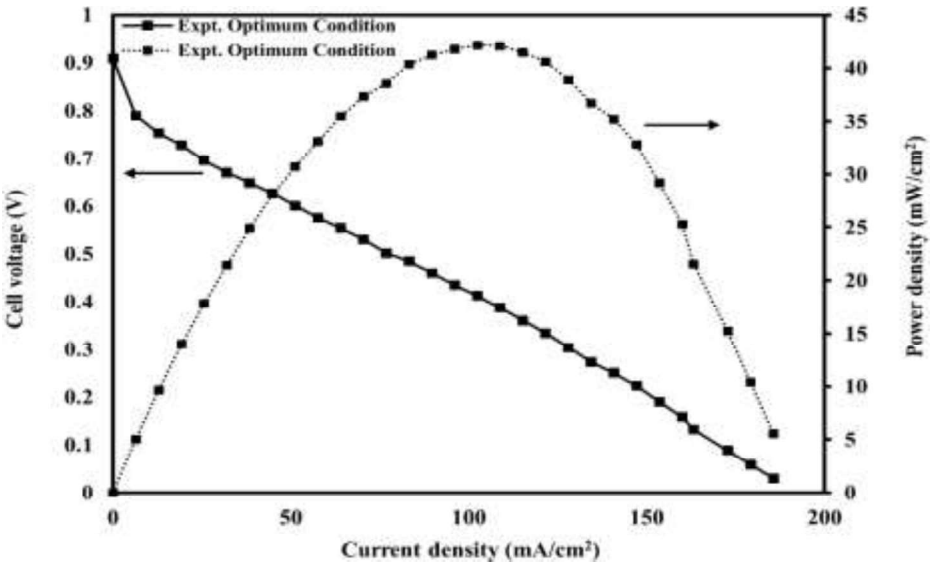

Figure 5.28a Current density vs. cell voltage and power density curves for optimum condition of cathode electrocatalyst loading of 1.12 mg/cm^2, cell temperature of 60.84 ^oC and hydrogen flow rate of 49.97 ml/min, Solid line – polarization curves; Dotted line – power density curves.

Table 5.15 Comparison of predicted and actual power density at the optimum condition obtained from the model.

Condition and criteria	Cathode loading (mg/cm^2)	Operating temperature (deg. C)	Hydrogen flow rate (ml/min)	Maximum Power density (mW/cm^2)	% error
Predicted	0.99	60.84	49.97	42.32	
Actual/Experimental	0.99	60.84	49.97	42.19	0.31

The maximum power density of 41.19 mW/cm^2 at a current density of 102.4 mA/cm^2 under the optimum conditions predicted by RSM analysis was achieved from the PEMFC experiment. Whereas, maximum model predicted power density at the same optimum condition was about 42.32 mW/cm^2. The % errors of power density between predicted and experimental value at optimum condition was 0.31 % found, which is in permissible limit.

The model equation for the response power density (Y) in Equation (5.6) was validated with experimental data by randomly assigning all operating parameters to certain values, namely, cathode electrocatalyst loading (A) of 1 mg/cm^2, cell temperature (B) of 55 ^oC and hydrogen flow rate (C) of 45 ml/min. Table 5.16 shows the experimental power density and predicted power density at the given random PEMFC operating conditions. The power density calculated from Equation (5.6) at random operating conditions was 36.36 mW/cm^2. However, the experimental value of maximum power density obtained under the identical random condition of PEMFC was 35.93 mW/cm^2. On comparing both predicted and experimental maximum power density between at random condition the % error was about 1.18 % (Figure 5.28b) and Table 5.16. It is clearly seen from the experimental validation of the developed RSM model reasonably filled.

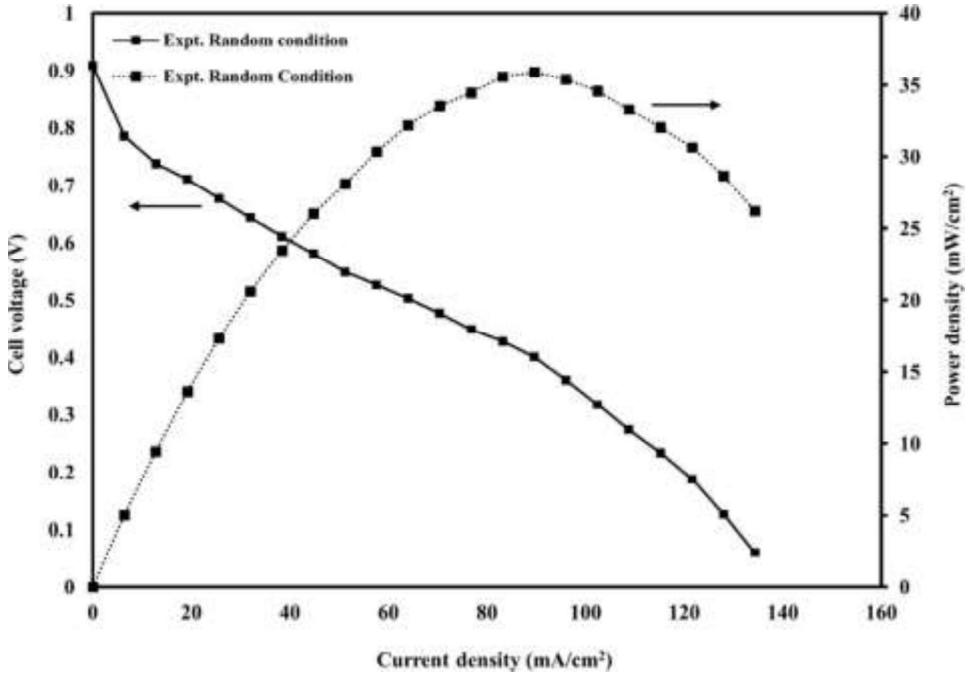

Figure 5.28b Current density vs. cell voltage and power density curves for optimum condition of cathode electrocatalyst loading of 1 mg/cm^2, cell temperature of 55 ^{o}C and hydrogen flow rate of 45 ml/min, Solid line – polarization curves; Dotted line – power density curves.

Table 5.16 Comparison of predicted and actual power density at the random condition obtained from the model.

Condition and criteria	Cathode loading (mg/cm^2)	operating temperature (deg. C)	Hydrogen flow rate (ml/min)	Power density (mW/cm^2)	% error
Criteria	In range	In range	In range	Maximum	Minimum
Predicted	1	55	45	36.36	
Actual/Experimental	1	55	45	35.93	1.18

5.2.5 Efficiency of the proton exchange membrane fuel cell (PEMFC)

The PEMFC efficiency was calculated for the electrocatalyst Pt-Co(3:1)/C_{AB}-EG and Pt-Ni(3:1)/C_{AB}-EG and using optimum condition at the room temperature of 33 ^{o}C. Proton exchange

membrane fuel cell efficiency is defined as the product of various individual efficiencies as given below (Carrette et al., 2001) in the Equation 5.7.

$$\eta_{FC} = \eta_r * \eta_V * \eta_F * \eta_U * \eta_H \quad (5.7)$$

Where, η_{FC} = Total efficiency
η_r= Thermodynamics efficiency
η_V = Electrochemical efficiency
η_U = Fuel utilization efficiency
η_F = Faraday efficiency
η_H = Heating value efficiency

The thermodynamic efficiency (η_r) is found from Gibbs free energy change (ΔG) and enthalpy change (ΔH) of the reaction involved and can be defined as ratio of the Gibbs free energy change (ΔG) to the enthalpy change (ΔH), of the reactions. The electrochemical efficiency (η_V) accounts for losses caused by electrode over potentials (activation and concentration overpotential) as well as resistive losses (electrolyte, interconnect, and contact resistances). It can be represented as the ratio of experimental OCV to the reversible cell potential (Carrette et al., 2001). The ratio of the actual number of electrons participating in the oxidation reaction (η_{actual}) to the theoretical maximum number of electrons involved in the whole fuel oxidation reaction (η_{Vtheo}) is expressed as faradaic efficiency (η_F). The actual fuel reacted when the fuel delivered to the fuel cell on a mass basis is characterized as the fuel utilization efficiency (η_F). It is assumed to be 0.95. (Larminie and Dicks 2003) because, the reaction does not use all of the fuel. Carrette et al., 2001 define heating value efficiency η_H as the ratio of the heating value of all fuel components transformed electrochemically to the heating value of fuel delivered in the fuel stream. Here, fuel is in pure form and thus, heating value efficiency is ignored in the present study.

Thus final form of equation 5.7 is obtained.

$$\eta_{FC} = \eta_r * \eta_V * \eta_F * \eta_U \quad (5.8)$$

Table 5.17 Efficiency of PEMFC using best Pt-Co(3:1)/-C_{AB}-EG and Pt-Ni(3:1)/C_{AB}-EG cathode electrocatalysts at room temperature (33 ^oC) and atmospheric pressure (1 atm).

Electrocatalyst type	η_r	η_V	η_F	η_U	η_{FC}
Pt-Co/C_{AB}-EG	0.96	0.72	0.80	0.95	52.53
Pt-Ni/C_{AB}-EG	0.96	0.74	0.80	0.95	53.99

The calculated efficiency of PEMFC for the Pt-Co/C_{AB}-EG and Pt-Ni/C_{AB}-EG cathode electrocatalyst were 52.23 % and 53. 99 %, respectively (Table 5.17). The PEMFC efficiency was slightly higher for the cathode electrocatalyst Pt-Ni/C_{AB}-EG than the Pt-Co/C_{AB}-EG.

5.2.6 Stability test using best cathode electrocatalysts Pt-Co(3:1)/C_{AB}-EG and Pt-Ni(3:1)/C_{AB}-EG in PEMFC

The best electrocatalysts Pt-Co/-C_{AB}-EG and Pt-Ni/C_{AB}-EG were only tested at a constant load when maximum power density was achieved for 12 hrs in hydrogen based PEMFC. As it is shown in Figure 5.29, operational cell voltage against maximum current density were recorded at equal intervals of 1 hr up to 12 hrs. The cell operational parameters were maintained at the optimum operational conditions obtained from the experimental studies in PEMFC. The operational voltage drop slightly from its initial voltage 0.4 V to 0.355 V after 12 hrs for electrocatalyst Pt-Ni(3:1)/C_{AB}-EG while, its falls more rapidly for cathode electrocatalyst Pt-Co(3:1)/C_{AB}-EG from 0.38 V to 0.33 V after 12 hrs in a same operation (Figure 5.29). The cell performance reduced slightly with time and it may be due to the poisoning of electrocatalyst sites.

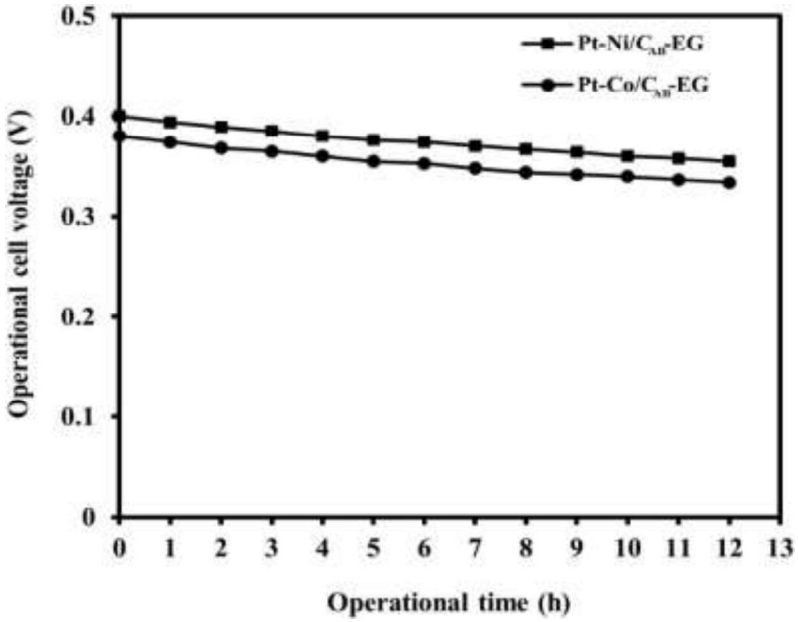

Figure 5.29 Stability test of hydrogen based PEMFC using the optimum conditions of operation at constant load at a temperature of 33 ºC for the best electrocatalyst Pt-Ni(3:1)/C_{AB}-EG and Pt-Co(3:1)/C_{AB}-EG.

Moreover, the catalyst layer is an integral part of the MEA for the fuel cell, its stability is essential for the lifespan of the fuel cell (Zhang et al., 2010). The deterioration process of the catalyst layer under the durability test was investigated using SEM. According to SEM images, before testing, the cathode catalyst layer had a comparatively smooth surface dispersed with Pt-Co(3:1)/C_{AB}-EG (Figure 5.30 (a)) and Pt-Ni(3:1)/C_{AB}-EG (Figure 5.30 (c)) electrocatalyst. However, the surface of the catalyst layer of Pt-Co/C_{AB}-EG (Figure 5.30 (b)) and Pt-Ni/C_{AB}-EG (Figure 5.30 (d)) becomes rougher than the original catalyst layer after 12 hours of operation (Song et al., 2021). Some pores collapse in some areas, reducing the number of accessible pores on the cathode electrode surface. Because of the increased agglomeration of electrocatalyst support material, it is implied that operation under complicated circumstances and at high temperatures degrades the microstructure of the catalyst layer (Song et al., 2021 and Strandberg et al., 2024). Therefore, the

SEM image in Figure 5.30 (d) also demonstrates that the Pt-Ni(3:1)/C_{AB}-EG catalyst is more stable than the Pt-Co(3:1)/C_{AB}-EG (Figure 5.30 (b)) catalyst in PEMFC.

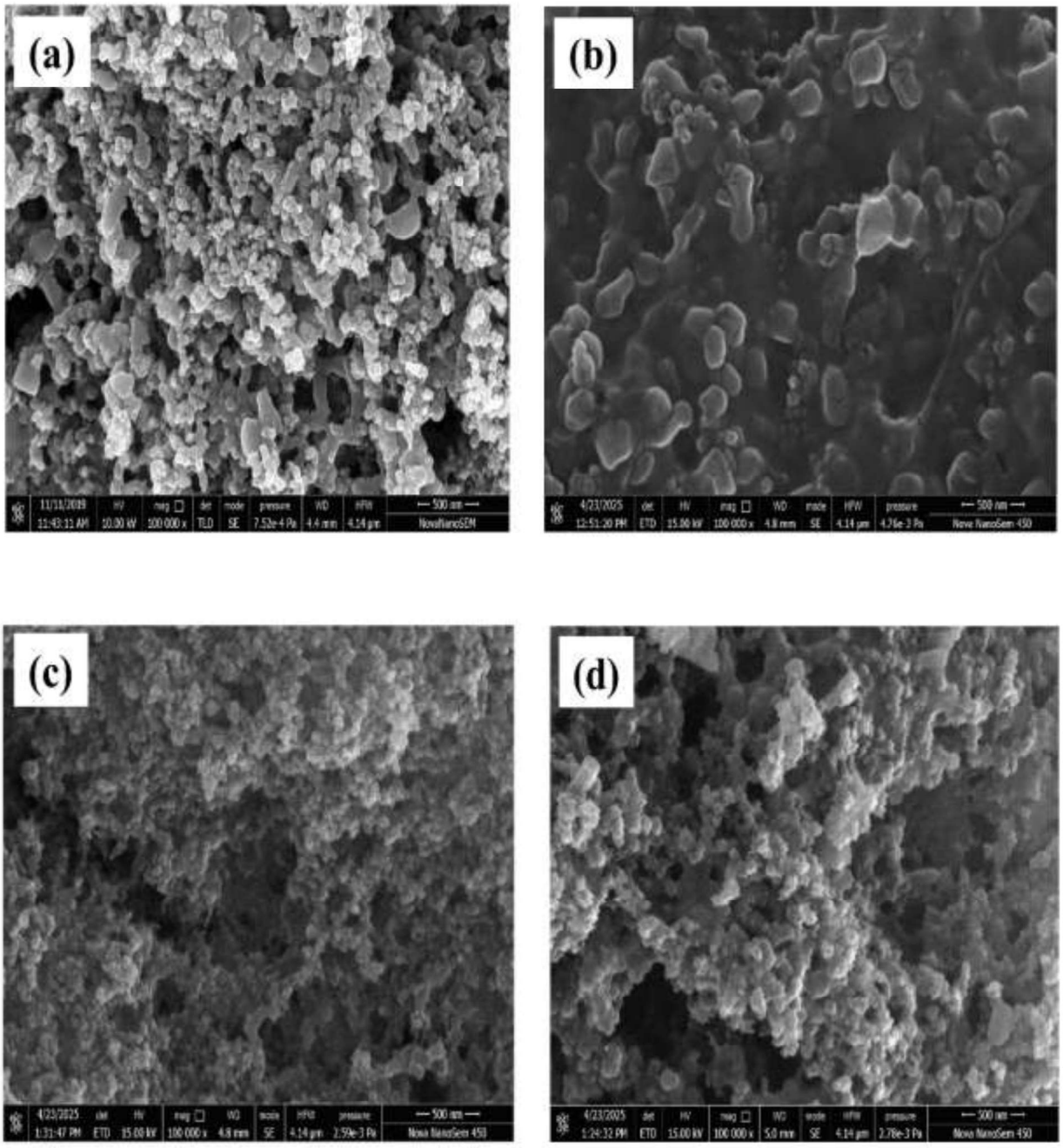

Figure 5.30 SEM images of (a) fresh Pt-Co(3:1)/C_{AB}-EG electrode, (b) used Pt-Co(3:1)/C_{AB}-EG electrode, (c) fresh Pt-Ni(3:1)/C_{AB}-EG electrode, and (d) used Pt-Ni(3:1)/C_{AB}-EG electrode.